

Chlorofluorocarbon uptake in a World Ocean model

2. Sensitivity to surface thermohaline forcing and subsurface mixing parameterizations

Matthew H. England¹

School of Mathematics, University of New South Wales, New South Wales, Australia

Anthony C. Hirst

Division of Atmospheric Research, Commonwealth Scientific and Industrial Research Organisation, Aspendale Victoria, Australia

Abstract. Part 1 of this study [England *et al.*, 1994] examined the sensitivity of simulated oceanic chlorofluorocarbon (CFC) to changes in the way the air-sea gas exchange rate is parameterized in a World Ocean model. In part 2 we consider more closely the role of surface thermohaline forcing and subsurface mixing parameterizations in redistributing CFC-11 and CFC-12 in the ocean. In particular, a series of five different model ocean experiments are forced with the same air-sea CFC flux parameterization. The five cases include (1) a control run with a standard seasonal cycle in surface forcing and traditional Cartesian mixing, (2) a run in which the production rate and salinity of Antarctic Bottom Water (AABW) is increased, (3) a run in which the production, outflow rates, and density of North Atlantic Deep Water (NADW) is increased, (4) a run with enhanced isopycnal mixing of passive tracers, and finally (5) a run in which the effects of eddies on the mean ocean flow are parameterized following Gent and McWilliams [1990]. The simulated CFC uptake in the Southern Ocean far exceeds observations in the first four experiments. The excessive uptake is linked to the poor model simulations of Southern Ocean deep water masses, where, for example, model Circumpolar Deep Water is typically 0.2 to 0.4 kg m^{-3} too buoyant. The insufficient density of the deep water allows for extensive penetration of convective adjustment to great depth during winter, in contrast to observations, and this results in excessive downward mixing of the CFC-enriched surface waters. Compared with the control experiment, the Southern Ocean CFC uptake is reduced in the cases with increased AABW salinity and NADW density, as a result of slightly higher deep water density and reduced wintertime convection in those experiments. Nevertheless, CFC uptake in the Southern Ocean still substantially exceeds observed ocean CFC content in the adjusted surface forcing cases. The most extreme uptake occurs in case 4, where, in addition to deep convective mixing of CFC, there is also mixing into the ocean interior along isopycnal surfaces having an unrealistic orientation. The Southern Ocean CFC uptake in case 5, using the mixing scheme of Gent and McWilliams [1990], is dramatically reduced over that in the other runs. Only in this run do deep densities approach the observed values, and wintertime convection is largely suppressed south of the Antarctic Circumpolar Current. Deep penetration of CFC-rich water occurs only in the western Weddell and Ross Seas. This run yields CFC sections in the Southern Ocean which compare most favourably with observations, although substantial differences still exist between observed and simulated CFC. The simulation of NADW production is problematic in all runs, with the CFC signature indicating primary source regions in the Labrador Sea and immediately to the southeast of Greenland, while the Norwegian-Greenland Sea overflow water (which is dominant in reality) plays only a minor role. Lower NADW is insufficiently dense in all runs. Only in the run with surface forcing designed to enhance NADW production does the CFC signal penetrate down the western Atlantic boundary in a realistic manner. However, this case exhibits an unrealistic net ocean surface heat loss adjacent to Greenland and so cannot be advocated as a technique to improve model NADW production. Conventional depth sections and volumetric maps of CFC concentration indicate that on the decadal timescales resolved by CFC uptake the dominant determining factor in overall model ventilation is the choice of subsurface mixing scheme. The surface thermohaline forcing only determines more subtle aspects of the subsurface CFC content. This means that the choice of subgrid-scale mixing scheme plays a key role in determining ocean model ventilation over decadal to centennial timescales. This has important implications for climate model studies.

¹Also affiliated with Division of Atmospheric Research, CSIRO, Aspendale, Victoria Australia.

1. Introduction

While temperature and salinity are routinely incorporated as prognostic variables in ocean circulation models, they are not ideal diagnostics of the ocean ventilation. This is because they provide only limited information on the rate of ocean re-

newal, such as indicating the depth of rapid ventilation associated with surface mixing. Yet the rate of ocean ventilation is among the most important properties relevant to the ocean's role in anthropogenic climate change. A rapidly ventilating ocean may be expected to be more efficient in sequestering excess heat and carbon from the atmosphere and thereby be more effective in retarding climate change. Despite the importance of ocean ventilation to the global climate system, there remains much uncertainty in the nature and timing of ocean renewal and how to represent this in general circulation models of the system.

Some of the most useful tracers for the study of oceanic ventilation on interdecadal timescales are the chlorofluorocarbons (CFC-11, CFC-12, CFC-113). These trace gases are chemically and biologically inert in the ocean and have well known histories of atmospheric concentration which extend from the 1930s (in the case of CFC-11 and CFC-12) to the present day. There is now a substantial set of observations of CFC distribution in the oceans, with many investigators using CFC concentrations to infer ventilation rates and pathways [e.g., Wallace and Lazier, 1988; Bullister, 1989; Rhein, 1991; Trumbore et al., 1991; Schlosser et al., 1991; Fine, 1993; Smethie, 1993; Roether et al., 1993]. However, only a few studies have examined the CFC distribution as simulated in ocean circulation models [England et al., 1994; England, 1995; Robitaille and Weaver, 1995; Dixon et al., 1996]. The goal of such studies is principally to test the model ventilation characteristics and to validate the model renewal scheme against observations.

Part 1 of this study [England et al., 1994] examined the dependence of modeled CFC uptake to a hierarchy of parameterizations of the air-sea CFC exchange. The ocean model was configured to have the same geometry and resolution as that used in several recent coupled ocean-atmosphere experiments [Manabe et al., 1991, 1992; Manabe and Stouffer, 1994]. All experiments performed in part 1 yielded CFC concentrations in the deep Southern Ocean that were very much higher than observed, implying that ventilation rates in the model Southern Ocean may be much greater than in reality. The rapid ventilation is largely associated with wintertime convective adjustment, which in the model is deep (several kilometres in places) and widespread. In reality, deep convection south of the Antarctic Circumpolar Current (ACC) appears to be weak, sporadic, and geographically very limited [e.g., Akitomo et al., 1995].

The question of ventilation in the Southern Ocean is important because models similar to that used in part 1 are being used in coupled ocean-atmosphere experiments designed to simulate the global climate response to steadily increasing levels of CO₂ [e.g., Manabe et al., 1991; Cubasch et al., 1992; Gordon and O'Farrell, 1997]. These simulations typically yield warming over the midlatitude and the subpolar southern hemisphere which markedly lags the warming in the tropics and northern hemisphere (as reviewed by Whetton et al. [1996]). It is possible that part of this retarded warming be linked to very rapid ventilation of the model Southern Ocean, which may not be entirely realistic [England, 1995; McDougall et al., 1996].

The excessive convection in the Southern Ocean appears to be linked to more general problems in model deep water simulation. Global ocean models frequently give deep water that is too fresh and/or warm and therefore too buoyant. For example, the deep water in the Southern, Indian, and Pacific Oceans in the model of England et al. [1994] is of order 0.3 practical

salinity units (psu) too fresh and 0.3 kg m⁻³ too buoyant (this is not unlike the climate model of Manabe et al. [1991], where deep waters are about 0.25 psu too fresh and 0.28 kg m⁻³ too buoyant). In contrast, the surface restoration of temperature and salinity keeps surface density near observed values across most of the Southern Ocean in England et al. [1994]. The result is a major weakening of the vertical stratification in the Southern Ocean, which in turn allows for excessive penetration of vertical convection [England et al., 1994]. Hirst and McDougall [1996] also give a detailed analysis of one such case.

Modelers have long been aware of this problem of insufficient saltness and density at depth, and one approach at correcting the solution has been to alter the surface boundary conditions at the locations where the deep water is originally formed. This can involve enhancing the salinity of Antarctic surface waters during winter in an attempt to mimic the effects of brine water rejection as sea-ice is formed [e.g., Bryan and Lewis, 1979; Cox, 1989; England, 1992, 1993; Hirst and Cai, 1994] or adjusting the wintertime thermohaline conditions in the North Atlantic to ensure the correct distribution of heat and salt when North Atlantic Deep Water (NADW) is produced [e.g., England, 1993; Hirst and Cai, 1994; Döscher et al., 1994]. Such adjustments in the thermohaline boundary conditions have been shown to improve the representation of deep water masses in global ocean models. However, their effects on the simulated ventilation rates remains largely unexplored and is one of the goals of the present study.

Limited by computational cost, climate studies require coarse resolution ocean models to permit simulations to be integrated over decadal to centennial timescales. The ocean's eddies are typically a fraction of the scale of grid spacing in ocean climate models. Techniques for parameterizing the sub-grid-scale model processes are therefore central to the global ocean modeling problem. The three major schemes for approximating the effects of eddies on tracers in the Geophysical Fluid Dynamics Laboratory (GFDL) ocean model are (1) to represent them as simple Fickian diffusion terms in the Cartesian plane, (2) to further incorporate an enhanced mixing of tracers in an along-isopycnal sense [Redi, 1982], and (3) to adopt the eddy-induced transport velocity terms of Gent and McWilliams [1990] and Gent et al. [1995]. In this paper we examine the details of transient tracer uptake when each of these three schemes is incorporated in a global ocean circulation model.

Some preliminary results from such experiments have been presented by England [1995]. Results similar to these have also been documented by Robitaille and Weaver [1995]. Our study considers a much more detailed analysis of CFC uptake than was possible in the papers of England [1995] and Robitaille and Weaver [1995], including analyses of air-sea CFC fluxes, examination of ocean CFC content at a greater variety of locations, and a volumetric temperature-CFC census of water masses in the different model cases.

Overall, we present results from a set of five experiments (Table 1) designed to assess the sensitivity of the model ventilation rate to changes in model physics or forcing which are known to affect the deep water density and extent of convection. To this end, we are able to determine which ocean model embellishments of the deep water mass field yield improved representation of transient ocean ventilation over the interdecadal timescale. In all model cases the ocean is run to (annual-cycle) equilibrium and then allowed to uptake CFC-11 and CFC-12 according to the observed atmospheric concentra-

Table 1. Experimental Design Adopted for the Present Study

Experiment	Integration Time (years)	Surface Forcing	Eddy Parameterization
CTRL	4750	Seasonally varying	Horizontal mixing (A_{HH})
AAS	3300	Increased S_* off Antarctica	Horizontal mixing (A_{HH})
NAW	3700	Strong winter restoring in NA	Horizontal mixing (A_{HH})
ISOP	3650	Seasonally varying	Isopycnal mixing, background A_{HH}
GM	4850	Seasonally varying	<i>Gent and McWilliams</i> [1990], $A_{HH} = 0$

Each model experiment is integrated until equilibration without using vertical acceleration techniques. The transient CFC simulations are then conducted over much shorter periods (around 65 years), corresponding with an integration during 1930–1995. In the table, S_* refers to the restoring surface salinity, and NA denotes the North Atlantic north of 45°N. The five cases listed are the control (CTRL), Antarctic Salt (AAS), North Atlantic Winter (NAW), isopycnal mixing (ISOP), and *Gent and McWilliams* [1990] (GM) experiments.

tion history and the most complete air-sea gas exchange scheme considered in part 1.

The rest of this paper is divided into six sections. In section 2 we describe the ocean model and experimental design adopted for the present study. The five model simulations are then detailed in section 3, with particular focus on the simulated density, vertical convection, and meridional overturning in the respective runs. In section 4 we briefly assess the sensitivity of heat and freshwater fluxes to the choice of surface T-S forcing. We then review the method used for parameterizing CFC exchange across the air-sea interface in section 5. Section 6 covers the analyses of CFC uptake within each case, concentrating on areas of deep and bottom water formation, as well as the implied surface air-sea CFC fluxes and the net content of CFC in each model case. Finally, section 7 covers a summary and concluding remarks.

2. Ocean Model and Experimental Design

The ocean model used in this study is the Modular Ocean Model (MOM) version of the Bryan-Cox ocean general circulation model developed at the Geophysical Fluid Dynamics Laboratory [Bryan, 1969; Cox, 1984; Pacanowski *et al.*, 1991]. The basic model configuration has been described in part 1 and by England [1993], and so only a summary is given here. The model geometry matches that used extensively within several recent coupled ocean-atmosphere model studies at the GFDL [e.g., Manabe *et al.*, 1991, 1992; Stouffer *et al.*, 1989]. The model domain consists of a global coverage of the World Ocean extending from the Antarctic continent to the north pole. The model bathymetry represents a smoothed version of the real World Ocean bottom topography. The model grid spacing is 3.75° longitude by approximately 4.5° latitude with 12 or 21 unequally spaced vertical levels.

The effects of mesoscale processes are taken into account implicitly by parameterizations of subgrid-scale mixing of momentum and tracers. The horizontal (A_{MH}) and vertical (A_{MV}) viscosity coefficients are taken to be constants independent of depth ($A_{MH} = 2.5 \times 10^9 \text{ cm}^2 \text{ s}^{-1}$; $A_{MV} = 50 \text{ cm}^2 \text{ s}^{-1}$). Model tracers (potential temperature (θ), salinity (S), CFC-11, and CFC-12) are subject to diffusion as detailed in Tables 1 and 2, as well as to advection. The vertical diffusivity (A_{HV}) is lowest in the surface layer ($0.3 \text{ cm}^2 \text{ s}^{-1}$), increasing below the thermocline (following Bryan and Lewis [1979]) toward a maximum of $1.3 \text{ cm}^2 \text{ s}^{-1}$ in the deeper model levels (Table 2). The horizontal diffusivity (A_{HH}) varies between experiments as described below. Convection is treated implicitly by the model; whenever gravitational instabilities in stratification are detected, the vertical diffusion rate is increased to simulate complete mixing over the unstable portions of the water column.

This vertical mixing homogenizes all tracers over the model levels originally detected to be dynamically unstable. No parameterization is included for deepening the surface mixed layer by wind-driven turbulence; that is, the convection of vertically unstable waters remains the only way deep mixed layers are formed in the model.

The ocean is forced at the sea surface by seasonally varying climatological boundary conditions of temperature, salinity, and wind stress. The atmosphere to ocean momentum flux is determined from the wind stress climatology of Hellerman and Rosenstein [1983] interpolated spatially onto the model grid and temporally at each time step. Except in the “North Atlantic Winter” experiment, temperature (T) and salinity (S) are damped toward the climatological values of Levitus [1982] with uniform restoring timescales of 30 days for T and 50 days for S . In all experiments considered, the ocean model is integrated with a fixed T-S time step of 1 day at all depths. The integrations continue until the equilibrium criterion of England [1993] is met, which in all cases requires 3000 to 4000 model years (Table 1).

The five principal experiments are listed in Table 1. The control experiment (CTRL) was used to examine the sensitivity of the CFC simulation to a range of air-sea gas exchange parameterizations in part 1. It adopts traditional Cartesian mixing with a horizontal diffusivity A_{HH} which decreases with depth ($A_{HH} = 1 \times 10^7 \text{ cm}^2 \text{ s}^{-1}$ in the surface level decreasing gradually toward $0.5 \times 10^7 \text{ cm}^2 \text{ s}^{-1}$ at depth [after Bryan and Lewis, 1979; Toggweiler *et al.*, 1989], Table 2). Surface T and S are restored to the climatological values of Levitus [1982] as indicated above.

The next two experiments examine the effect of changes to the surface thermohaline forcing on the interior ocean ventilation pattern. Several investigators have been able to achieve fairly realistic deep and bottom water properties by setting the restoration salinity to high values (34.8 to 35.0 psu) at a limited number of grid points adjacent to Antarctica (see Toggweiler and Samuels [1995] for a review). The “Antarctic Salt” (AAS) experiment examines the impact of using such a technique. It differs from the control only in that the restoring salinity is increased to 35.00 psu for all ocean grid boxes at latitudes 77.8°S and 73.4°S during three wintertime months (i.e., the two southernmost latitude rows, similar to England [1993]). We also reduce the salinity restoring timescale to only 10 days during the winter months to ensure high salinities during this period. The peak wintertime shelf water salinity increases from 34.41 psu in CTRL to 34.95 in AAS, and this greatly enhances the density and production rate of the model’s Antarctic Bottom Water (AABW). We anticipate that this may in turn act to restrict deep convection to the southernmost grid points in the Weddell and Ross Seas, so possibly

Table 2. Vertical Grid Spacing and the Vertical, Horizontal, and Isopycnal Mixing Coefficients used in the Model Runs

Level	ΔZ	Z	A_{HV}	A_{HH}	A_p
1	50.9	50.9	0.305	0.98×10^7	4.80×10^7
2	68.4	119.3	0.306	0.92×10^7	4.37×10^7
3	100.4	219.7	0.307	0.86×10^7	3.85×10^7
4	151.1	370.8	0.310	0.78×10^7	3.22×10^7
5	224.0	594.8	0.314	0.69×10^7	2.52×10^7
6	319.6	914.4	0.321	0.61×10^7	1.88×10^7
7	432.5	1346.9	0.339	0.55×10^7	1.42×10^7
8	551.0	1897.9	0.393	0.52×10^7	1.16×10^7
9	660.9	2558.8	0.887	0.51×10^7	1.05×10^7
10	751.9	3310.7	1.236	0.50×10^7	1.01×10^7
11	820.4	4131.1	1.280	0.50×10^7	1.00×10^7
12	868.9	5000.0	1.300	0.50×10^7	1.00×10^7
1	50.9	50.9	0.305	0.98×10^7	4.80×10^7
2	61.4	112.3	0.306	0.92×10^7	4.40×10^7
3	73.6	185.9	0.307	0.87×10^7	3.97×10^7
4	85.9	271.8	0.308	0.82×10^7	3.53×10^7
5	99.0	370.8	0.310	0.76×10^7	3.10×10^7
6	107.5	478.3	0.312	0.71×10^7	2.71×10^7
7	116.5	594.8	0.314	0.67×10^7	2.37×10^7
8	143.8	738.6	0.317	0.63×10^7	2.05×10^7
9	175.8	914.4	0.322	0.60×10^7	1.77×10^7
10	194.6	1109.0	0.328	0.57×10^7	1.53×10^7
11	237.9	1346.9	0.339	0.54×10^7	1.34×10^7
12	263.0	1609.9	0.357	0.53×10^7	1.21×10^7
13	288.0	1897.9	0.393	0.52×10^7	1.12×10^7
14	317.2	2215.1	0.496	0.51×10^7	1.07×10^7
15	343.7	2558.8	0.886	0.51×10^7	1.03×10^7
16	360.9	2919.7	1.162	0.50×10^7	1.02×10^7
17	391.0	3310.7	1.236	0.50×10^7	1.01×10^7
18	404.0	3714.7	1.264	0.50×10^7	1.00×10^7
19	416.4	4131.1	1.280	0.50×10^7	1.00×10^7
20	425.8	4555.9	1.289	0.50×10^7	1.00×10^7
21	444.1	5000.0	1.295	0.50×10^7	1.00×10^7

Grid box thickness (ΔZ) and depth of the base of each model level (Z) are shown for both the 12 and 21 level cases. Also shown are values of the vertical (A_{HV}), horizontal (A_{HH}), and isopycnal (A_p) diffusivities adopted. Mixing parameters are fixed in experiments CTRL, AAS and NAW (with $A_p = 0$). In ISOP, A_p is nonzero (taking values as shown above), and A_{HH} is constant ($0.75 \times 10^7 \text{ cm}^2 \text{ s}^{-1}$). In experiment GM, A_{HH} is zero everywhere, and the extra mixing term of Gent *et al.* [1995] is included (with $\kappa = 1 \times 10^7 \text{ cm}^2 \text{ s}^{-1}$).

reduce the overall ventilation rate and CFC uptake of the Southern Ocean. However, Toggweiler and Samuels [1995] have criticized this method because it might require unrealistically large heat and freshwater fluxes over the Antarctic seas. Their model was unfortunately carried out with annual mean forcing conditions even though previous studies [e.g., England, 1993] restrict the adjusted salinity condition to three wintertime months. We shall therefore also examine the Antarctic surface fluxes of this and other runs.

Details of the thermohaline forcing in the North Atlantic can also have a significant effect on the deep density of the Southern Ocean [England, 1993]. This is because the NADW flowing southward out of the Atlantic basin contributes substantially to the Circumpolar Deep Water (CDW), which is the major subsurface water mass south of the ACC. The lower NADW in the model of England *et al.* [1994] is too buoyant by about 0.3 kg m^{-3} . This discrepancy partly results from peak wintertime densities of surface water in the subpolar North Atlantic falling well short of observed values (because of the finite timescale for surface restoration in conjunction with a large annual cycle of surface density and other factors). In the

second experiment, "North Atlantic Winter" (NAW), the surface densities are forced to be close to climatological values by using a very short restoration timescale over the North Atlantic. The experiment differs from CTRL only in that the restoring coefficient for both T and S is reduced to $(10 \text{ days})^{-1}$ in the Atlantic Ocean and associated seas north of 45°N , during three wintertime months. The shorter timescale on surface restoring ensures genuine wintertime conditions in the far North Atlantic, with surface waters becoming realistically cold and saline. For example, peak surface density (σ_θ) in the Greenland-Norwegian Sea increases from 27.74 kg m^{-3} in CTRL to 27.98 kg m^{-3} in experiment NAW, which is nearly identical to the peak wintertime value of 27.97 kg m^{-3} implied from the Levitus [1982] climatology. Consequently, the density and production rate of NADW is substantially increased.

The next two experiments feature introduction of parameterizations for the effect of mesoscale eddies. In the first such experiment, "Isopycnal Mixing" (ISOP), the widely used scheme of M.D. Cox (unpublished manuscript, 1987) is adopted to include the effect of tracer diffusion along the isopycnal surfaces. This scheme has been shown to have only a minor effect on the deep density field [England, 1993; Hirst and Cai, 1994] but is included here because it creates additional pathways for penetration of CFC into the ocean interior (by diffusion along the isopycnal surfaces). Specifically, the ISOP experiment differs from the control only in that a mixing of tracers is included along the isopycnal surfaces [after Redi, 1982; M.D. Cox, unpublished manuscript, 1987], and the horizontal diffusivity is changed to a constant value of $A_{HH} = 0.75 \times 10^7 \text{ cm}^2 \text{ s}^{-1}$. This represents a decrease in horizontal diffusivity in the upper 370.8 m, although an increase in the deeper model levels. This is in contrast to other studies whereby the depth profile of horizontal diffusivity is decreased uniformly when isopycnal mixing is adopted [e.g., Cummins *et al.*, 1990; England, 1993; Böning *et al.*, 1995]. However, we have chosen to follow the choice of isopycnal and horizontal diffusivity exactly as in the study of Manabe *et al.* [1991, 1992] in order to make direct comparison with their model. While the value of A_{HH} is constant in ISOP, the isopycnal diffusion decreases with depth between surface and deep values ($5.0 \times 10^7 \text{ cm}^2 \text{ s}^{-1}$ in the surface layer gradually decreasing to $1.0 \times 10^7 \text{ cm}^2 \text{ s}^{-1}$ at depth; Table 2).

The final experiment, "GM", features the scheme of Gent and McWilliams [1990] and Gent *et al.* [1995] for representing adiabatic transport effects of baroclinic eddies. The results of Danabasoglu *et al.* [1994], England [1995], Danabasoglu and McWilliams [1995] and Hirst and McDougall [1996] demonstrate that use of this scheme results in marked increases in the deep water density and an associated reduction in convection. Some of these studies indicate improvements in the steady state simulation of deep temperature and salinity, although the sensitivity of transient ventilation rates to the scheme has only been partly explored [Duffy *et al.*, 1995; England, 1995; Robitaille and Weaver, 1995; McDougall *et al.*, 1996].

Specifically, the GM experiment differs from the control in that (1) a parameterization is included for the effects of eddy-induced transport as per Gent and McWilliams [1990] and Gent *et al.* [1995], (2) an isopycnal tracer diffusivity is included as per experiment ISOP, (3) the horizontal diffusivity is set to zero, and (4) the number of model levels is increased to 21. It may be noted that the eddy-induced velocity of the Gent *et al.* [1995] method is not in fact due to bolus advection. Rather, as

has been shown by *McDougall and McIntosh* [1996], the extra advection that is provided by the two-dimensional streamfunction of the *Gent and McWilliams* [1990] method, when added to the resolved-scale Eulerian velocity of an ocean model, yields the temporal-residual-mean velocity. *McDougall et al.* [1996] have pointed out that this implies that the eddy-induced velocity is due to the sum of the bolus velocity and the difference between the velocity averaged at constant density and at constant height.

The implementation of the *Gent et al.* [1995] parameterization is as detailed by *Hirst and McDougall* [1996]. The diffusivity which determines the strength of the eddy-induced transports is set at $1.0 \times 10^7 \text{ cm}^2 \text{ s}^{-1}$ [after *Danabasoglu et al.*, 1994; *Hirst and McDougall*, 1996; *Rix and Willebrand*, 1996]. A highly desirable feature of the *Gent et al.* [1995] parameterization is that it allows the model to be run with small or zero horizontal diffusivity. There is little physical justification for inclusion of horizontal diffusivity [e.g., *McDougall and Church*, 1986], and it is retained in the other experiments solely to ensure numerical stability. It has been shown to significantly degrade model solutions, for example, by facilitating unrealistically large diapycnal fluxes of buoyancy and by inducing large diapycnal volume transports [e.g., *Veronis*, 1975; *Böning et al.*, 1995; *Hirst et al.*, 1996]. We increase the number of model levels here in order to achieve the level of numerical stability found necessary to run the model without horizontal diffusivity. The model levels for the GM experiment are listed in Table 2 and are chosen in such a way as to ensure that no changes to the model topography were necessary (since all model bathymetric features are at least 370.8 m deep). The ISOP and CTRL experiments were also rerun with the 21 levels used in GM, with little change in results for CFC uptake and overall model ventilation rates.

Ocean models which employ the *Gent et al.* [1995] scheme and have zero horizontal diffusivity frequently display some locally pronounced numerical noise. Under certain conditions, more serious numerical distortion of the tracer fields appears to occur (e.g., see examples discussed by *Hirst and McDougall* [1996]). The present GM experiment may provide a useful test in this regard because CFC concentrations should not be less than zero, so development of any regions with negative CFC concentration indicate tracer field contamination problems. In our CFC integration under GM the strongest negative values of CFC at any given level are at most 8% of the principal CFC signal at that depth (similar magnitude negative values are found in CTRL though not in ISOP). This indicates only minor numerical distortion of the penetrating CFC signal under GM.

3. Circulation, Density, and Convection in the Model Experiments

Three properties of the ocean simulation of particular interest are the circulation, vertical convection, and the shape of interior density surfaces. Together these three parameters define the deep ocean uptake rate of CFC in the model experiments. While all model cases are ventilated as a function of the vertical convection and interior ocean currents, the shape of density surfaces also influences interior CFC mixing rates in experiments ISOP and GM. Overall, the model ocean ventilation is determined by convection, mixing, and vertical velocity in regions of water mass formation and, in addition, by

the interior circulation and diffusion in regions not directly renewed by water at the sea surface.

A synthesis of vertical and horizontal motion is found in a map of the model meridional overturning. Exact ventilation rates must, however, be calculated from the exact velocity fields since the timescale for ocean circulation is determined not by net transport rates but by ocean current speeds. Nevertheless, the merging of two circulation aspects in the one map makes the meridional overturning a useful diagnostic of our model ocean circulation. Along with the convection patterns in the model and the shape of isopycnal surfaces in experiments ISOP and GM, CFC distributions can be largely explained in terms of these three circulation diagnostics.

Two caveats should be mentioned concerning vertical tracer communication in the model. First, the model parameterization of convection does not strictly involve a circulation; tracers are mixed vertically outside any calculation of vertical motion. Second, the vertical motion itself is not a prognostic variable of the model; it is simply determined diagnostically through the continuity equation.

3.1. Meridional Overturning

Figure 1 shows the meridional overturning streamfunction in experiments CTRL, AAS, NAW, and GM for the globe (upper panel) and the Atlantic sector (lower panel). That for experiment ISOP is little changed from the control and so is not shown. Key features for all five experiments are also summarized in Table 3. Compared to the control run, the increased wintertime salinity forcing in experiment AAS leads to enhancement of the direct Antarctic cell (centered near 65°S and 2000 m depth) and to a lesser extent the deep cell (centered near 20°S and 3200 m depth). These cells are associated with AABW production and outflow. The AABW is much saltier and denser than in the control run, and this strongly affects salinity and density of the deep ocean (Table 3, see also *England* [1993]). However, the remainder of the overturning circulation appears only slightly affected.

The increased wintertime North Atlantic forcing in experiment NAW leads to a much enhanced overturning circulation in the Atlantic, with the outflow of NADW more than doubling that in the control run. There is some weakening of the direct Antarctic cell in this case. The outflowing NADW is also much denser, with θ and S at the core of the Deep Western Boundary Current at 30°S changing from the control by up to -1.38°C and $+0.33 \text{ psu}$, respectively. This change in output volume and density (up to 0.16 kg m^{-3}) again substantially increases the density of the deep ocean (Table 3). The enhanced NADW outflow partly suppresses the inflow of WSBW in the Atlantic sector (dropping from 5.3 to 3.2 Sv, Table 3). The AABW production rate also drops (by 6.4 Sv) in response to the enhanced NADW outflow. Overall, we might expect an increase in advection of the CFC signal into the deep Southern and North Atlantic Oceans, respectively, for the cases AAS and NAW, on the basis of changes in the meridional overturn alone.

The effective transport velocity (i.e., resolved Eulerian velocity plus eddy-induced transport velocity) is used to calculate the overturning streamfunction for experiment GM (Figures 1g and 1h), since this quantity is the most relevant to the redistribution of tracers. The resulting pattern of overturning is qualitatively quite different to that in the other four cases. As expected from *Gent et al.* [1995], *Danabasoglu et al.* [1994], and

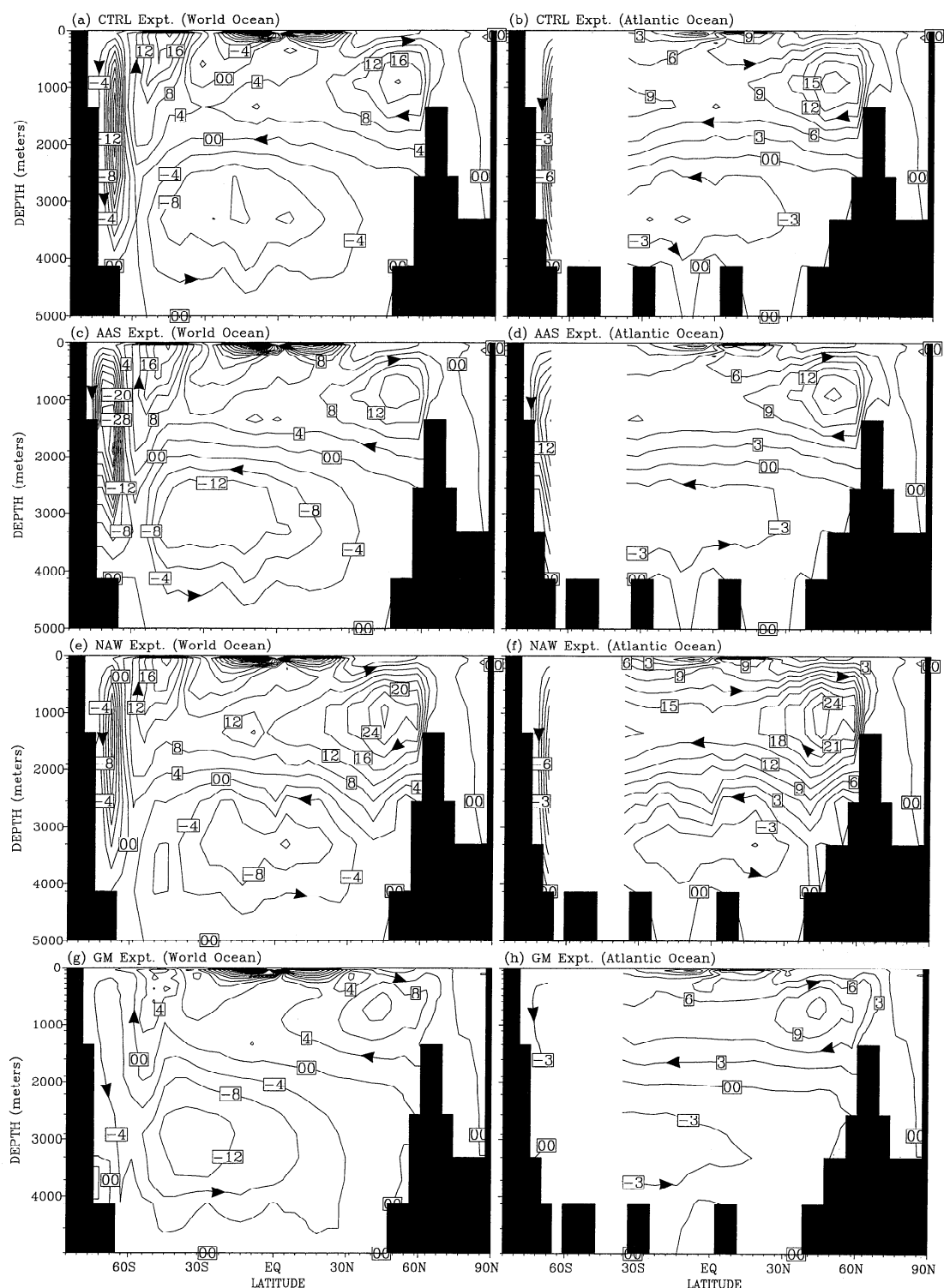


Figure 1. Annual mean global meridional overturning (Sv , $1 \text{ Sv} = 10^6 \text{ m}^3 \text{ s}^{-1}$) in experiments CTRL, AAS, NAW, and GM. Also shown is the overturning streamfunction in the Atlantic sector. No contours are drawn in the Atlantic Ocean where the model is zonally unbounded. Contours are drawn at 4 Sv and 3 Sv intervals, respectively. Meridional overturning values shown for experiment GM include the additional tracer advection transports of *Gent et al.* [1995].

Danabasoglu and McWilliams [1995], the Deacon cell is very weak (because the indirect cell of the resolved Eulerian transport is partly cancelled by a direct cell resulting from the eddy-induced transport). Also, the direct Antarctic cell is dramatically weakened and now appears as an extension of the deep

cell. Further, the Atlantic overturning circulation weakens moderately, and the outflow of NADW shoals (it should be noted, however, that the eddy advection terms act to enhance the NADW production and outflow rates by about 1-2 Sv; it is the resolved Eulerian overturning that weakens in GM com-

Table 3. Selected Circulation and Water Mass Properties of the Five Ocean Experiments

Experiment	NADW (Production)	NADW (Outflow)	AABW (Production)	WSBW (Atlantic)	ACC, Sv	θ_{10} °C	S_{10} psu	$\sigma_{0,10}$ kg m ⁻³	$\sigma_{3,10}$ kg m ⁻³
CTRL	20.1	8.5	30.9	5.3	148	2.24	34.43	27.52	40.94
AAS	18.4	6.8	41.2	6.2	159	2.26	34.69	27.73	41.13
NAW	28.5	17.3	22.1	3.2	131	2.81	34.60	27.61	40.98
ISOP	19.3	8.1	29.4	5.2	142	1.24	34.26	27.46	40.95
GM	12.9	6.9	7.6	4.4	101	-0.19	34.44	27.69	41.29
Observed	17.0	15.0	15.0	5.0	134	1.51	34.74	27.83	41.29

The production rates of NADW and AABW are defined as the maximum overturning rates in the North Atlantic and Antarctic thermohaline cells, respectively. The outflow of NADW is defined as the rate of outflow of water of North Atlantic origin across the latitude at the southern tip of South Africa (32°S). The table also indicates the amount of Weddell Sea Bottom Water (WSBW) that flows into the Atlantic sector and recirculates under NADW (e.g., Figure 1). Meridional overturning values shown for experiment GM include the additional tracer advection transports of *Gent et al.* [1995]. The ACC transport is defined as that flowing through the Drake Passage, while (θ_{10} , S_{10}) is the global-mean θ - S signature simulated at level 10 (i.e., 2935 m depth). Global mean in situ ($\sigma_{3,10}$) and potential ($\sigma_{0,10}$) density at 2935 m depth are also shown. Values shown at 2935 m depth in experiment GM are obtained by interpolation of neighboring model levels (Table 2). Observed estimates of these parameters are also included (deep and bottom water formation rates taken from *Schmitz* [1995] and *Rintoul* [1991]; ACC transport is from *Nowlin and Klinck* [1986], and hydrographic parameters are from *Levitus* [1982]).

pared with ISOP). In view of these changes in the global meridional overturning we would expect advection of the CFC signal into the ocean interior to be weaker in experiment GM than in the other cases.

3.2. Deep Water Density and Stratification

The occurrence of convection is, of course, governed by the stratification of the water column, and there are major changes in stratification between the experiments. Figure 2a shows profiles of potential density averaged over the Southern Ocean between 50°S and 65°S for each experiment and from the *Olbers et al.* [1992] climatology. Panel 2b shows the corresponding mean depth profiles of CFC-11 in each of the five model experiments during 1994. The control and isopycnal mixing runs show unrealistically weak stratification in the upper 1500 m of the water column in the region, primarily because of insufficient density of the interior water (Figure 2a). This permits extensive surface water convective overturn in these cases (see section 3.3), enabling high levels of CFC uptake in these runs (Figure 2b). There is a clear correspondence between weak stratification and high CFC content in the model experiments, indicating the importance of convective overturn in ventilating the model Southern Ocean on annual to decadal timescales.

While surface densities are little changed between the runs (because of the local surface restoration), AAS, NAW, and GM display substantial increases in the subsurface density, and thus strengthened stratification, over that in CTRL. This is particularly the case for experiment GM, whose density profile most closely resembles the shape and magnitude of the observations (though it should be noted this is achieved largely by compensating errors in deep T and S; Table 3). The subsurface density increases in the AAS and NAW runs reflect input of much denser AABW and NADW, respectively, resulting from the isolated changes in surface forcing in those cases. Despite the relatively weak overturning in GM, all deep water types (including NADW) are considerably denser in this experiment than in the control run. The increase in the GM case is characteristic of runs employing the *Gent and McWilliams* [1990] scheme and results from elimination of horizontal diffusivity and other factors [*Danabasoglu et al.*, 1994; *Duffy et al.*, 1995; *Danabasoglu and McWilliams*, 1995; *Hirst and McDougall*,

1996]. Such changes in stratification have a substantial effect on the extent of convective adjustment.

In experiments ISOP and GM the orientation of density surfaces influences interior mixing rates (through the isopycnal mixing scheme of *Redi* [1982]). Plate 1 shows a zonal mean of the estimated trajectories followed by isopycnal tracer diffusion in the Southern Ocean (the model's neutral surfaces [*McDougall*, 1987]). The neutral surface trajectories are estimated following the method of *Reid* [1981, 1989], where surfaces are assumed to follow contours of potential density referenced to the surface in the upper 540 m, to 1500 m over the interval 540 m to 2300 m, and to 3000 m at depths below 2300 m. Also shown are the corresponding neutral surfaces from the *Olbers et al.* [1992] climatology of the Southern Ocean. Superposed on the density surface maps are the concentrations of oxygen (observed annual mean [*Olbers et al.*, 1992]) and CFC-11 (simulated annual mean during 1994).

In experiment ISOP, isopycnal surfaces are spuriously steep in the Southern Ocean in the upper 1500 m, with little vertical stratification south of 50°S. This permits a pathway of rapid vertical penetration of surface water properties compared with the real ocean. The climatological map (Plate 1a) shows markedly flatter isopycnal surfaces, with older oxygen-depleted CDW upwelling from the north at this latitude, with a strong vertical stratification of density layers in the surface 500 m. The oxygen signal suggests little downward penetration of surface waters at 50°S to 70°S. Experiment GM exhibits a more realistic neutral surface orientation in the Southern Ocean. Density layers are flatter, and this inhibits vertical penetration by isopycnal mixing in the circumpolar region.

3.3. Vertical Convection

In the context of CFC uptake simulations the convective activity of the model is somewhat more important than the meridional overturning. This is because the timescale for convective adjustment in the ocean (hours to days) is much more rapid than the timescale for vertical motion. For example, the vertical motion (or meridional overturning) requires just over 30 years to take some surface level information (e.g., newly introduced CFCs) to 1000 m depth, based on a generous scale vertical velocity of 10^{-6} m s⁻¹. Convection in the model effi-

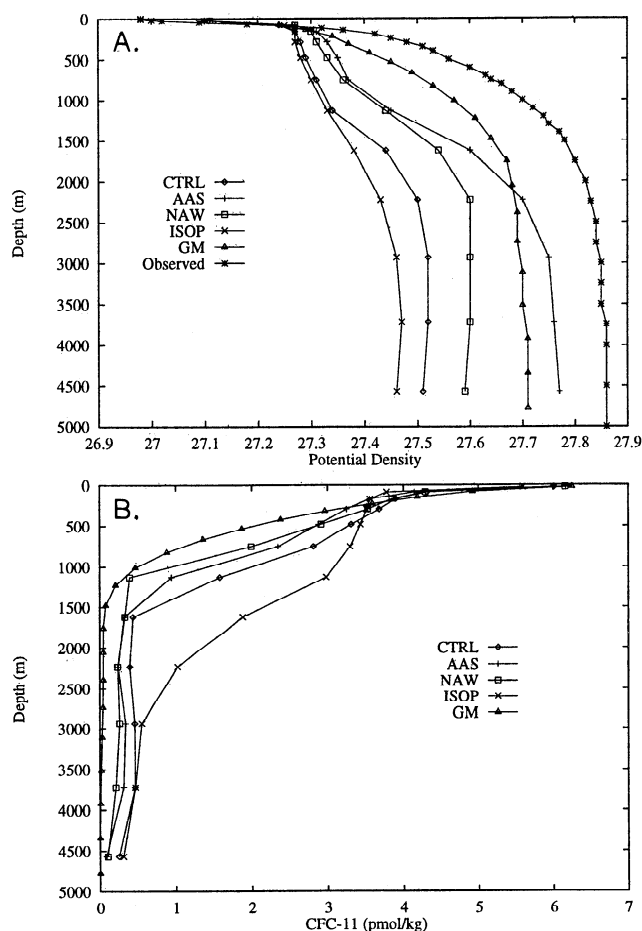


Figure 2. (a) Mean depth profile of potential density averaged over the Southern Ocean between 50°S and 65°S for each experiment and from the *Olbers et al.* [1992] climatology. (b) Mean depth profile of CFC-11 between 50°S and 65°S in each of the five model runs during 1994. There is insufficient CFC data to construct such a profile from observations.

ciently homogenizes entire unstable water columns during just one time step (i.e., just over 1 day). The meridional overturning maps are more relevant, in the CFC context, for showing ventilation rates from regions of convective activity (e.g., the outflow rate of NADW).

Figure 3 shows the maximum surface layer convection depth in four of the five experiments over the World Ocean (convection in the ISOP experiment is very similar to the CTRL case, *England* [1995], and so is not shown here). The maps are derived from determination of the depth attained by convective adjustment from the surface at each time step during an annual cycle of the equilibrated model runs. Included in Figure 3d and the analysis for the ISOP case are those regions where the slope of the isopycnal surfaces exceeds 1 part in 100 (corresponding to the maximum slope set for isopycnal diffusion), which generates vertical diffusion terms that partly replace explicit convective mixing [*Hirst and Cai*, 1994]. The first four cases all show extensive deep convection in the Southern Ocean. In AAS the wintertime influx of salt leads to very deep convection in the far south Ross and Weddell Seas, with the resulting denser deep water inhibiting some convection in the Southern Ocean (near 60°S; Figure 3b). The denser inflow of NADW in case NAW yields only a very minor reduction in convective activity in the Southern Ocean from that in CTRL. The convection in ISOP is also little changed, which is

again consistent with the relatively minor effect that the isopycnal tracer diffusion has on the density field.

The widespread deep convection found in these cases between 55°S and 70°S conflicts with observations, which show that this band is mostly characterized by upwelling of old CDW and shallow surface mixed layers [e.g., *Olbers et al.*, 1992] (Plate 1a). This striking discrepancy between observed and modeled circulation in the Southern Ocean is likely to generate quite erroneous CFC distributions. In contrast to the above cases, convection in the GM case is largely limited to the Antarctic shelf and north of the polar frontal zone (both thought to be regions of convective mixed layer formation [e.g., *McCartney*, 1977; *Killworth*, 1983]).

The pattern of convection in the North Atlantic varies less between the cases than that in the Southern Ocean. Cases CTRL, AAS, and ISOP all yield similar patterns. North Atlantic convection is slightly stronger in the NAW case, with maximum convective mixed layer depths increasing from 1347 m (CTRL) to 1898 m (NAW) in the Greenland Sea. Similar increases in convection depths are noted elsewhere in NAW. Convective overturn is moderately weaker in the GM case, with somewhat shallower penetration of convective instability and a general reduction in the extent of the convection area. For example, convection in the Labrador-Greenland Seas contracts to a small area off southeast Greenland (with a maximum depth of convection of only 739 m). Reduced convection in GM is due to a general densification of deep and bottom waters in that model run, leading to enhanced upper ocean stratification and shallower winter mixed layers.

The above patterns mostly reflect the depth achieved by late winter convection. Also important in CFC penetration is the duration of convection during the course of the year. For example, under the *Wanninkhof* [1992] gas flux parameterization, CFC-11 concentrations in a column of well mixed water 1000 m deep approach saturation via the surface gas flux with a timescale of around 300 days (assuming a typical wind speed of 10 m s⁻¹ in waters of temperature 0–5°C). Clearly, subsurface CFC concentrations in such a column will much more quickly increase toward saturation if convective mixing occurs all year, rather than just for a few weeks each year. Figure 4 shows summertime (July–September, northern hemisphere; January–March, southern hemisphere) maximum depth of convection for CTRL, AAS, NAW, and GM cases. The CTRL case shows that deep convection continues in parts of the North Atlantic and Southern Oceans even in summer. In NAW the relatively dense subsurface water created during wintertime results in much reduced convection in the northern hemisphere during the remainder of the year. Similarly, Ross and Weddell Sea convection is largely limited to wintertime months in experiment AAS (in contrast to CTRL and NAW). Case ISOP (not shown) has a pattern similar to that of CTRL. The GM case yields almost no summertime convection deeper than 120 m.

The marked overall reduction in convection in the GM case is broadly consistent with the findings of *Danabasoglu et al.* [1994], *Danabasoglu and McWilliams* [1995], and *Hirst and McDougall* [1996]. Together with the generally reduced rate of overturning and slope of isopycnal surfaces, we may anticipate that CFC penetration in this case will be significantly less than in the other four experiments.

4. Heat and Freshwater Flux Sensitivity to Surface T-S Forcing

Adjusting the surface thermohaline forcing conditions in experiments AAS and NAW will affect the implied heat and

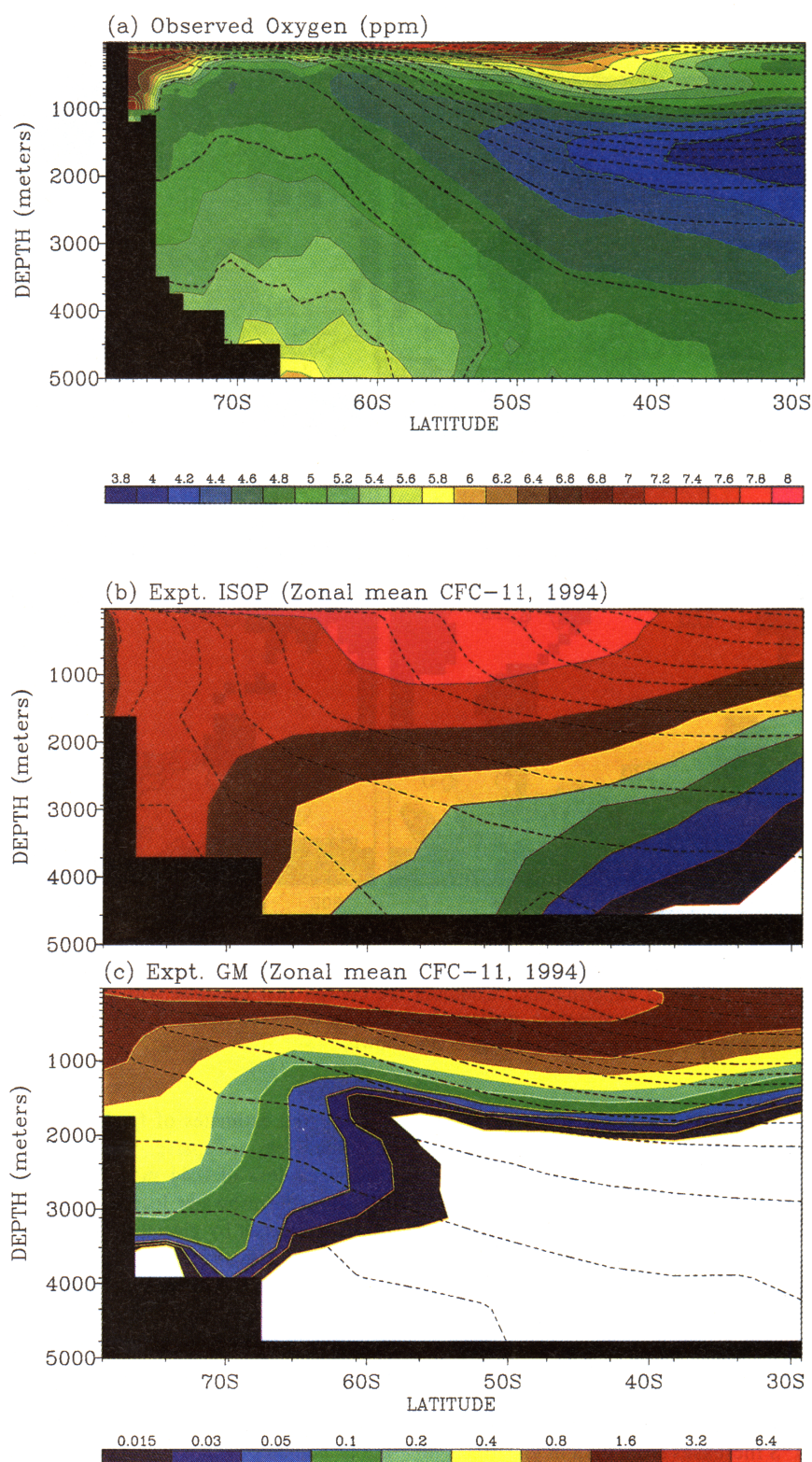


Plate 1. Zonal mean neutral surface trajectories estimated following the method of Reid [1981, 1989]. Surfaces are assumed to follow contours of potential density referenced to the surface in the upper 540 m, referenced to 1500 m over the interval 540 to 2300 m, and referenced to 3000 m at depths below 2300 m. (a) From the Olbers *et al.* [1992] climatology of the Southern Ocean, (b) experiment ISOP, and (c) experiment GM. Superposed on the density surface maps are the concentration of dissolved oxygen (observed annual mean [Olbers *et al.*, 1992]) (Plate 1a) and the annual mean CFC-11 simulated during 1994 in experiments ISOP and GM (Plates 1b and 1c).

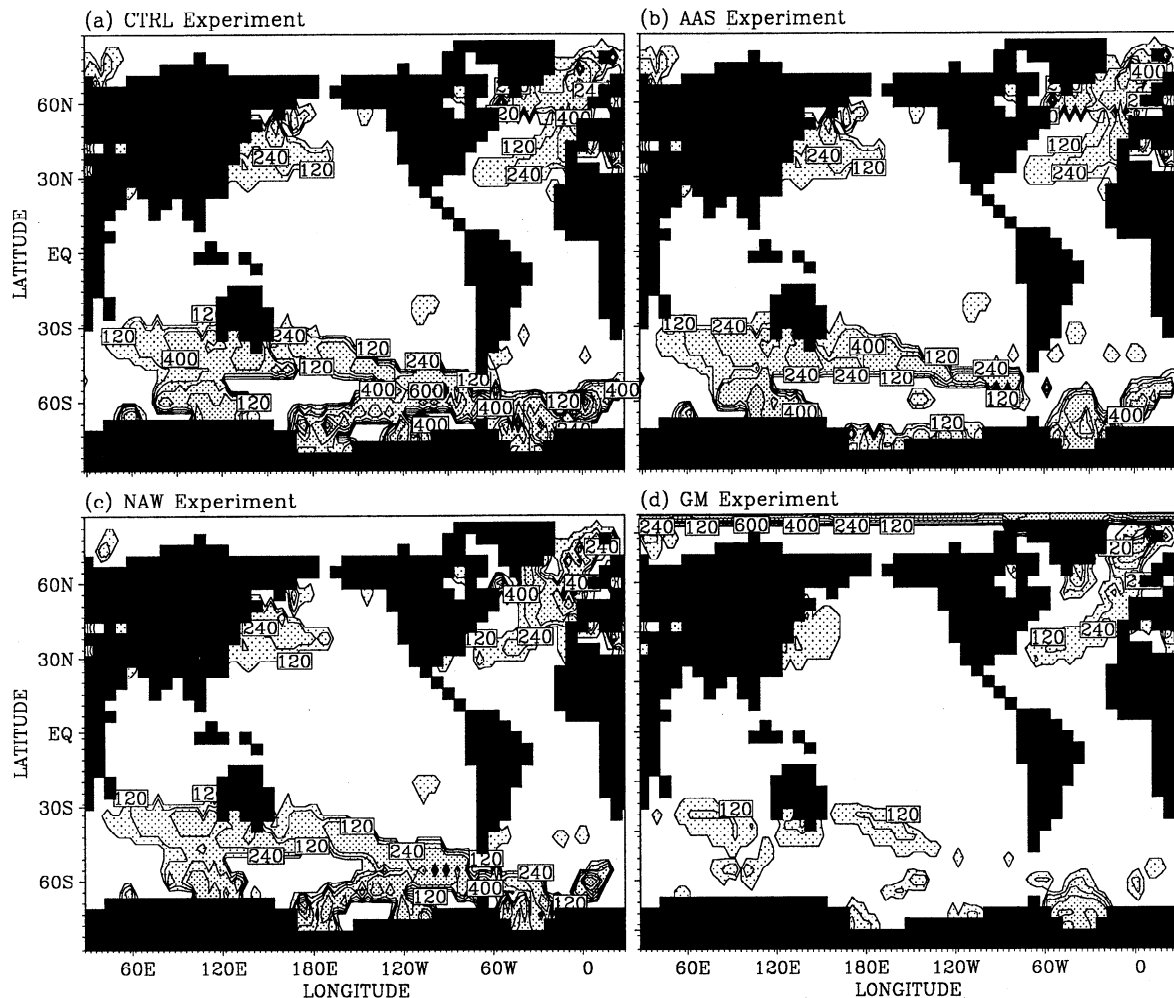


Figure 3. Maximum depth of surface level convective overturn (in meters) during a complete annual cycle of the equilibrated ocean model experiments. Contours are chosen that coincide with successive model level depths. Regions of convective overturn greater than 120 m (i.e., the upper 3 model levels) are shaded. Experiment ISOP is very similar to CTRL and so is not shown.

freshwater fluxes at the air-sea interface. It is important to examine to what degree the new surface fluxes are in agreement with observations. Figure 5 compares the implied freshwater fluxes in experiments CTRL and AAS over the far Southern Ocean, as well as the surface heat fluxes in CTRL and NAW over the northern North Atlantic.

Changing the restoring salinity off Antarctica in AAS during three wintertime months implies a higher net freshwater loss in that experiment. The effective freshwater flux adjacent to Antarctica is balanced by interior ocean export of saline surface water (primarily by convection and lateral diffusion). The area-weighted mean net freshwater export from the Weddell (Ross) Sea south of 71°S increases from 0.15 m yr^{-1} (0.02 m yr^{-1}) in CTRL to 2.90 m yr^{-1} (1.99 m yr^{-1}) in AAS. However, it should be noted that the regions of high net freshwater loss in AAS are concentrated in only a few model grid points in the eastern Ross and Weddell Seas (Figure 5b), where the model bathymetry is quite deep. High freshwater loss is required here to balance very deep convective overturn of saline water during wintertime. Future studies are planned to examine the impacts of Antarctic salt adjustments when they are more realistically limited to the continental shelves of the Ross and Weddell Seas.

Observed estimates of freshwater export from the Weddell and Ross Seas are sparse. *Jacobs et al.* [1985] estimate a net freshwater loss of 0.44 m yr^{-1} for the Ross Sea; made up of 0.95 m yr^{-1} freshwater loss due to the formation and removal of sea ice, offset by glacial meltwater (0.36 m yr^{-1}) and precipitation minus evaporation (0.15 m yr^{-1}). *Zwally et al.* [1985] estimate much greater rates of sea-ice formation (4.6 to 7.8 m yr^{-1} for the entire Antarctic shelf); while recent coupled ice-atmosphere models suggest an annual mean freshwater loss of order 1 m yr^{-1} for both the Ross and Weddell Seas [e.g., *Wu et al.*, 1997].

It therefore appears that under a Cartesian mixing scheme the technique of enhancing Antarctic salinities can lead to spurious freshwater fluxes, particularly when the enhancement occurs over deep regions of the model domain. In a previous study, *England* [1993] used a similar salt flux technique in a model with isopycnal mixing and a more substantial recirculation of saline CDW in the Southern Ocean. In that case, an annual mean freshwater loss of only 0.55 m yr^{-1} was diagnosed for waters south of 71°S . The lower values of implied freshwater loss in that case are likely to be due to the higher near-shelf salinities of upwelled CDW (thereby reducing the required fluxes to maintain high surface salinities during winter), as

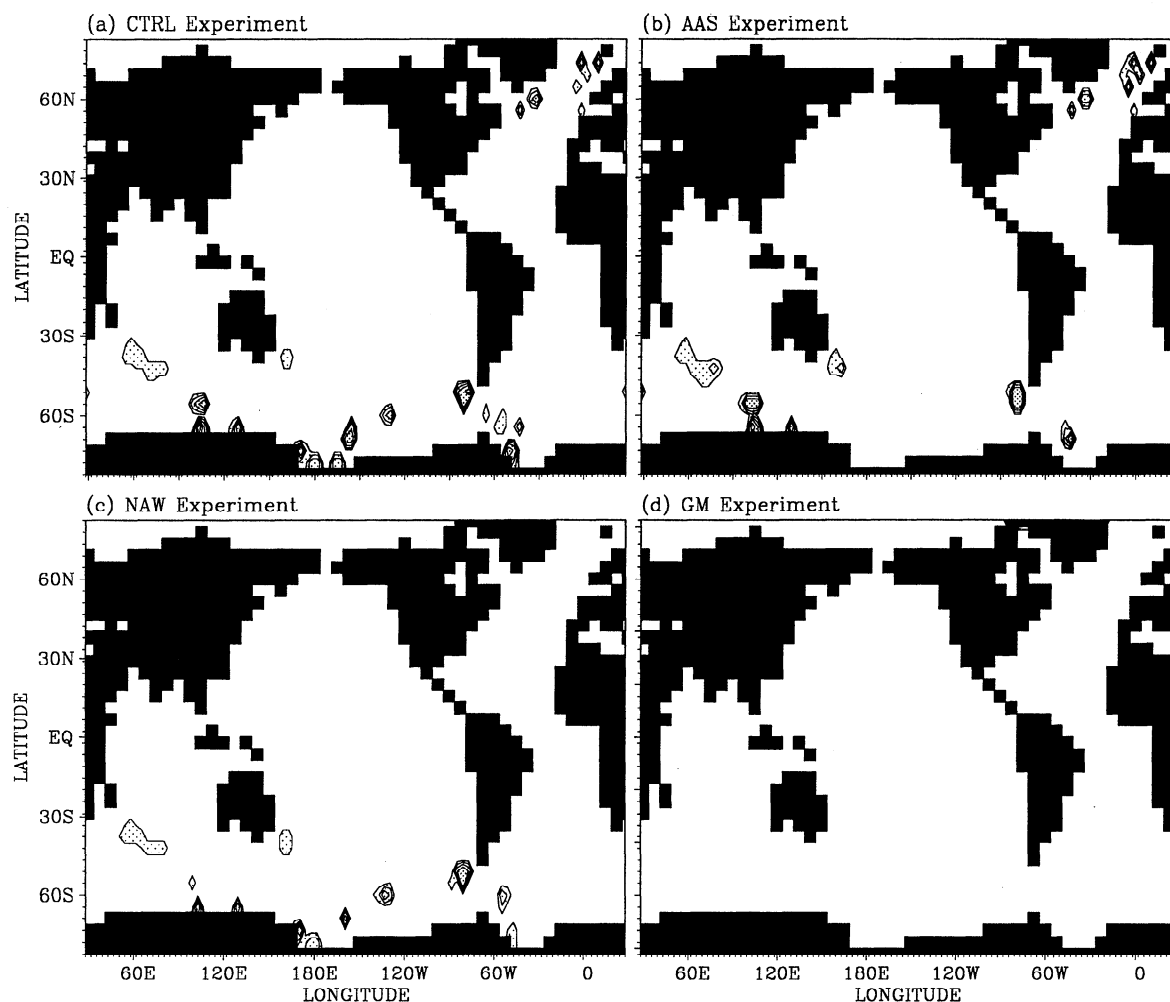


Figure 4. As in Figure 3, only showing maximum depth of surface level convective overturn (in meters) during summertime months (July–September in the northern hemisphere, January–March in the southern hemisphere).

well as reduced lateral mixing (which weakens the removal of high salinity shelf water by unrealistic horizontal diffusion).

The shorter wintertime restoring timescale used in experiment NAW greatly enhances North Atlantic surface heat fluxes in that model run. Annual and regional mean net surface heat loss in the Greenland and Labrador Seas is substantially increased in NAW. Compared with a maximum annual mean surface heat loss of order 90 W m^{-2} in the climatology of *Esbenson and Kushnir* [1981], the NAW experiment loses as much as 730 W m^{-2} in an isolated grid point south of Greenland (Figure 5d). In comparison, CTRL exhibits a more smoothly varying field of implied surface heat loss, with a relative annual mean maximum of 186 W m^{-2} southeast of Greenland. In summary, experiment NAW requires artificially high net surface heat fluxes to maintain near-observed T-S during wintertime months in the North Atlantic.

5. Including CFC Uptake in the Model

To run a simulation of CFC uptake, we take the equilibrated ocean circulation model (typically derived from a 3000- to 4000-year integration) and restart the integration with two additional tracers (CFC-11 and CFC-12) initially at zero concentration everywhere. The model is then run nominally from

year 1930 until the end of 1995 with an uptake of the atmospheric gases CFC-11 and CFC-12. The industrial release of these gases began in the early 1930s and accelerated greatly during the next 3 decades [see *England*, 1995, Figure 1]. Despite the discovery that CFCs destroy stratospheric ozone [*Molina and Rowland*, 1974], the atmospheric concentration of these gases has continued to rise until recently [*Elkins et al.*, 1993]. Even though virtually all production and release of CFCs has occurred in the northern hemisphere, rapid mixing rates in the lower atmosphere and the chemical stability of CFCs ensure relatively uniform distributions of these gases over the troposphere. We assume that the latitudinal variation of atmospheric CFC concentration is small enough to be approximated by a function of hemisphere and time (Figure 1 in part 1).

The forcing of CFC fluxes in the present study is similar to the most realistic case presented in part 1 (i.e., experiment “CF4”). The parameterized uptake of CFC-11 and CFC-12 follows the physical law governing air-sea gas exchange, namely,

$$Q = k(\alpha C_{\text{atm}} - C_w) \quad (1)$$

where Q is the gas flux across the air-sea interface (fluxes from the atmosphere into the ocean are positive), k is the gas transfer speed, α is the solubility coefficient of the given gas, C_{atm}

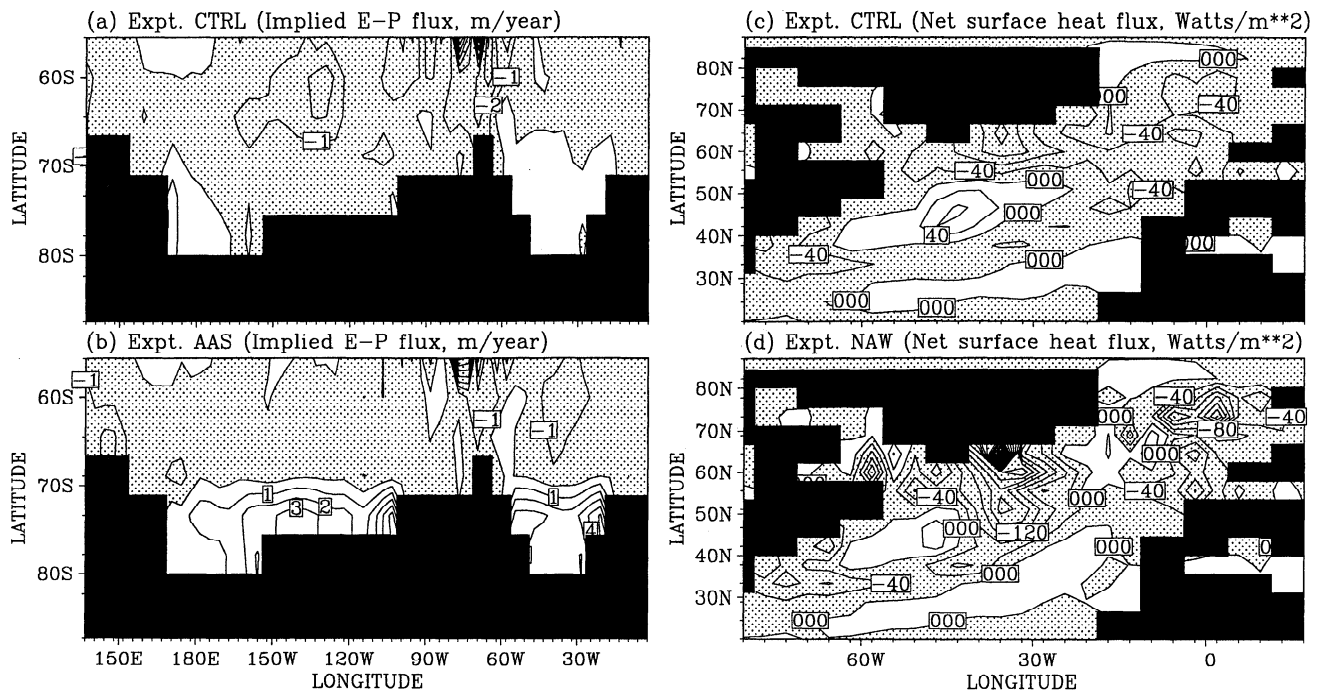


Figure 5. (a) and (b) Diagnosed annual mean freshwater fluxes (in meters per year) in experiments CTRL and AAS over the far Southern Ocean. (c) and (d) Diagnosed annual mean surface heat fluxes (in Watts per square meter) in experiments CTRL and NAW over the northern North Atlantic. Stippled regions denote a surface freshwater gain in Figures 5a and 5b and a surface heat loss in Figures 5c and 5d.

is the atmospheric concentration over the sea surface, and C_w is the concentration of the given gas in the near-surface seawater. For a gas whose seawater and atmospheric concentrations are known, and whose solubility properties are understood, calculating the gas flux simply requires a parameterization of the gas transfer velocity k . In the present series of gas uptake experiments, k is parameterized according to the relation (following Wanninkhof [1992] with an additional sea-ice factor)

$$k = k_0 u^2 [1 - R] / \sqrt{Sc} \quad (2)$$

where k_0 is a constant (7.964) derived from bomb-produced radiocarbon invasion rates into the ocean (which includes implicitly the Schmidt number for ^{14}C), u is the climatological wind speed (in meters per second), R is the fraction of sea-ice cover (derived from Parkinson *et al.* [1987] and Comiso *et al.* [1993]), and Sc is the Schmidt number for the given gas. In the calculation of k we reference the Esbenson and Kushnir [1981] seasonally varying wind speeds and compute Sc as a function of climatological temperature for each gas. That is, k varies seasonally on account of seasonal changes in the surface wind speed, sea-ice cover, and upper level temperature (through its determination of the Schmidt number Sc).

The solubilities of CFC-11 and CFC-12 in seawater have been derived experimentally by Warner and Weiss [1985]. In moist air and at a given pressure (assumed to be constant at 1 atm) the solubility of CFC-11 and CFC-12 varies as a function of temperature and salinity, though in seawater the temperature dependence greatly outweighs the influence of salinity. We reference the seasonal T and S climatology (not the predicted model T-S) to compute the *in situ* solubility of CFC-11 and CFC-12. This is done to ensure that each of the five ocean states has the same reference saturation levels of CFC-11 and CFC-12. Actual surface level concentrations will then vary ac-

cording to differences in simulated convection and vertical motions. Differences in surface level temperature between the cases will not directly affect the upper level CFC concentration through the solubility term, only indirectly through its influence on convection and vertical motion patterns. Extensive tests reveal that using the seasonal T-S climatology (as opposed to the model predicted T-S) to compute the solubility of CFC results in order 5-8% higher (lower) upper ocean CFC concentrations during winter (summer), due largely to a damping of the seasonal cycle by the model thermohaline forcing.

In part 1 it was shown that the wind speed dependent parameterization of surface CFC exchange reproduced many of the subtle variations in upper ocean saturation levels, namely, undersaturation in regions of deep convective overturn and near-surface upwelling and supersaturation in the summer mixed layer. In addition, the sea-ice factor realistically limits the air-sea gas transfer in direct proportion to the observed seasonally varying sea-ice coverage (see part 1). As has been explained above, in spite of the variations in ocean conditions between experiments, a controlled surface forcing has been adopted to minimize the uncertainties in analyzing the different CFC simulations from one experiment to the next. This includes using identical *in situ* solubility distributions, wind speeds, sea-ice coverage, and Schmidt numbers in each of the five experiments. Variations in the CFC simulations then result only as a function of differing vertical overturn and circulation between the respective experiments.

6. CFC Uptake in the Ocean Model Experiments

6.1. Air-Sea CFC Fluxes

Figure 6 shows the annual mean air-sea flux of CFC-11 in each of the five model experiments during 1983, as well as a

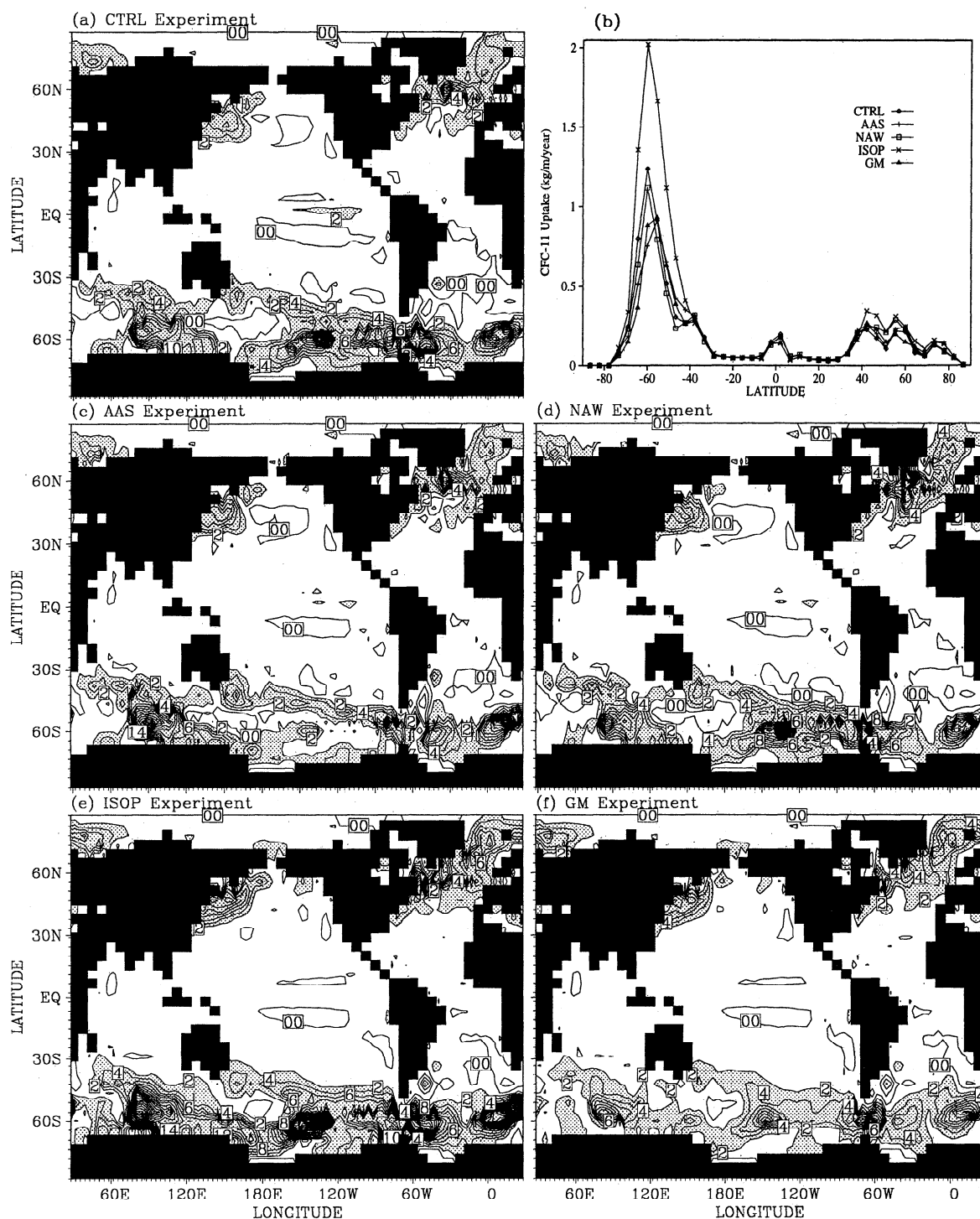


Figure 6. Annual mean air-sea CFC-11 flux in each of the five model experiments during 1983, as well as a panel showing the corresponding globally integrated CFC uptake as a function of latitude. Contour interval is $2 \text{ pmol kg}^{-1} \text{ yr}^{-1}$. Stippled regions denote a net ocean CFC-11 uptake in excess of 2 pmol kg^{-1} during 1983. The global-integral values are obtained from a zonal integral of the surface gas fluxes in $\text{pmol kg}^{-1} \text{ yr}^{-1}$; converted to an amount of CFC-11 uptake in $\text{kg m}^{-1} \text{ yr}^{-1}$ noting that the molecular weight of CFC-11 (CCl_3F) is 137.36 gmol^{-1} , the density of surface seawater is order 1025 kg m^{-3} , and the depth of the upper model level is 50.9 m .

panel showing the corresponding globally integrated CFC uptake as a function of latitude. Spatial variations in CFC uptake are similar in other years because the pattern of ocean uptake is determined by the model ocean circulation and convection structure, which exhibit little interannual variability. The net

globally integrated uptake of CFC-11 evolves as a function of the atmospheric history of the gas and the model ocean circulation patterns. Apart from small interseasonal variations (due to the seasonally varying ocean overturn cycle), the net CFC uptake broadly increases with time.

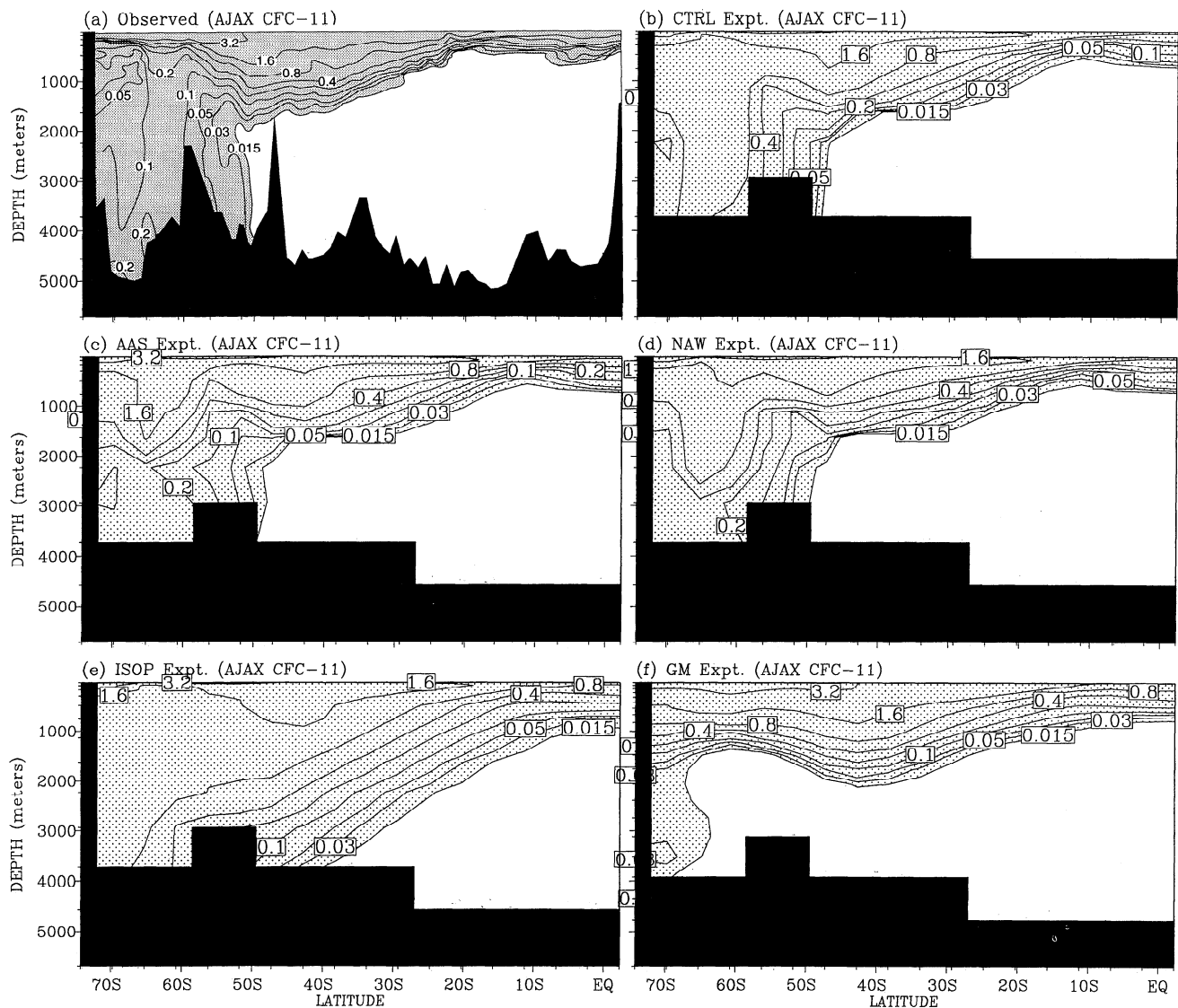


Figure 7. Latitude-depth sections of dissolved CFC-11 along the prime meridian during late 1983. (a) Observed (redrafted from Warner and Weiss [1992]) and (b)-(f) experiments CTRL, AAS, NAW, ISOP, and GM. To be consistent with observational studies, contour levels are drawn at 0.015, 0.03, 0.05, 0.1, 0.2, 0.4, 0.8, 1.6, and 3.2 pmol kg^{-1} .

A comparison with Figure 3 indicates that the pattern of CFC surface exchange is substantially tied to the pattern of convection. Convection results in the rapid mixing of CFC-rich surface water with CFC-deficient subsurface water, with consequent reduction of surface CFC concentration and so a large air to sea flux of CFC. An exception occurs in all cases in the Ross and Weddell Seas, where extensive sea-ice cover limits air-sea CFC exchange, despite the occurrence of deep convection. The CFC flux into the Southern Ocean appears reduced in the AAS case from that in CTRL, in part because of reduced convection north of 70°S and in part because the very intense convection associated with the wintertime salinity enhancement occurs in regions of high coverage of sea-ice. The ISOP experiment exhibits the strongest air-sea CFC fluxes over the Southern Ocean due to rapid overturn of surface waters by either explicit vertical convection or relatively rapid mixing along steeply sloping isopycnal surfaces (see also Plate 1b).

CFC fluxes are substantially reduced in the GM case, especially in the Southern Ocean as expected on the basis of reduced convection and meridional overturn. However, significant uptake in this case clearly extends beyond the limits of penetrative convection (Figure 3d), with upwelling of old CFC-deficient water and mixing along sloping isopycnal surfaces playing a significant role in maintaining below-equilibrium surface CFC concentrations near 55° to 70°S.

6.2. CFC Uptake in the Southern Ocean

The modeled CFC distributions in the Southern Ocean are examined in this section with reference to observed sections of CFC concentration across the Southern Ocean. Figure 7 shows observed and modeled CFC-11 concentrations along the Ajax section (October 1983 to January 1984), lying roughly at the Greenwich meridian [Warner and Weiss, 1992]. The modeled concentrations are the mean values during late 1983 (October

through December). Clearly evident in Figure 7b is the excessive penetration of CFC in CTRL, especially to the south of about 55°S. The high concentration (~1 pmol kg⁻¹) throughout the water column east of the Weddell Sea is a direct result of deep convection which in places extends nearly to the deep ocean floor. In contrast, observed concentrations in excess of just 0.3 pmol kg⁻¹ are restricted to the upper 200 m at Weddell Sea latitudes. The AAS and NAW experiments (Figures 7c and 7d) show significant reduction in CFC penetration at depths greater than about 2000 m, but concentrations at lesser depth remain excessive. Implementation of isopycnal tracer diffusion in case ISOP (Figure 7e) clearly degrades the CFC distribution further from that in CTRL. In all other cases, some representation of the observed CFC minimum associated with CDW is evident, but in ISOP this feature is totally lost. Experiment GM also displays excessive ventilation in the upper 1000 m, but CFC concentrations at greater depths are dramatically reduced over those in all other runs and are in fact less than observed. The contrast between GM and ISOP is particularly marked, even though both cases include isopycnal tracer diffusion.

The role of convection and isopycnal tracer diffusion in determining ocean ventilation characteristics is further illustrated in Plate 2, which shows modeled CFC along the South Atlantic Ventilation Experiment (SAVE) Section G near 25°W–35°W (January–April, 1989) superposed on estimates of the trajectories followed by isopycnal tracer diffusion (namely, the model's neutral surfaces [McDougall, 1987]). For the purposes of this diagram the SAVE-G section (which was taken southward to 55°S [Weiss *et al.*, 1993]) is extended southwestward into the Weddell Sea. No CFC data can therefore be presented south of 55°S in the observed panel. The neutral surface trajectories are estimated following the method of Reid [1981, 1989], where surfaces are assumed to follow contours of potential density referenced to the surface in the upper 540 m, to 1500 m over the interval 540 m to 2300 m, and to 3000 m at depths below 2300 m. Overlaying the observed SAVE-G CFC-11 are the corresponding neutral surfaces from the Levitus [1982] climatology of the World Ocean.

In the ISOP case (Plate 2b), extensive outcropping of deeply penetrating neutral surfaces occurs in the Southern Ocean and Weddell Sea. In contrast, the observed deep ocean is much denser than in ISOP (Figure 2), and deep-ocean neutral surfaces estimated from climatological T and S (Plate 2a) do not outcrop in the open ocean. Thus the isopycnal tracer diffusion in ISOP creates an additional and unrealistic pathway for penetration of CFC into the ocean interior. In addition, horizontal tracer diffusion is nonzero ($0.75 \times 10^7 \text{ cm}^2 \text{ s}^{-1}$) in ISOP, yielding an additional diffusion scale distance of about 500 km in 10 years. With such steeply sloping isopycnal surfaces in the Southern Ocean in ISOP this translates to a strong diapycnal flux of CFC-11, enabling excessively rapid blending of the tracer signal.

In the GM case (Plate 2c), deep ocean density is greater, and deep-ocean neutral surfaces realistically do not outcrop over the open ocean but instead only over the shelf at a few points in the southernmost Ross and Weddell Seas. Thus the very low values of deep CFC in the GM case reflect the absence of deep convection and the weakness of advection and isopycnal diffusion of CFC from off the Antarctic continental shelves. In addition, a clear signal of CFC-depleted CDW is simulated in GM, whereas case ISOP shows no such depletion. While both cases have an advective signal of recirculating CDW at this lat-

itude, only GM has sufficiently weak diapycnal mixing to inhibit the CFC signal from contaminating the older CDW. In addition, there is much weaker isopycnal mixing downward and northward into the older CDW as a result of much more limited outcropping of the relevant isopycnal surfaces in GM. This agrees well with the observed structure of CFC-11 penetration at SAVE section G.

Figure 8 shows CFC concentrations for the SR3 section across the Southern Ocean at approximately 150°E in 1991. The observed section (Figure 8a) shows deepest penetration at about 45°S, with only very shallow penetration between about 55°S and 65°S. A very thin band of recently formed AABW is found adjacent to the Antarctic continental slope. None of the cases capture the band of AABW well, as is expected for a model of such coarse resolution. Otherwise, cases CTRL, AAS, and NAW give excessive ventilation south of about 55°S, and ISOP again gives severely excessive ventilation at most latitudes. Only the GM solution appears to fairly closely reproduce the observed CFC distribution; particularly the strong vertical gradients in CFC observed at 55°S to 65°S along SR3.

The overall meridional ventilation of the Southern Ocean is summarized in Plate 1 for observations and cases ISOP and GM. This figure includes modeled zonal mean CFC-11 content in the Southern Ocean in 1994 overlaid with contours representing the model's approximate neutral surfaces (as discussed previously). For comparison, the observed annual mean oxygen climatology of Olbers *et al.* [1992] is also shown. Both the observed panel and the GM simulation show old waters upwelling from 1000 to 4000 m depth at 40°S into the upper part of the Southern Ocean near 50°–70°S. As has been discussed previously, this is CDW which is observed to be largely depleted of CFC (e.g., Figure 7a, Plate 2a, and Figure 8a). In contrast, case ISOP exhibits rapid Southern Ocean ventilation at all latitudes. Runs CTRL, AAS, and NAW (zonal mean figure not shown) also show higher than observed CFC uptake in the Southern Ocean. Of all the experiments, case GM captures the most markedly depleted signal of CFC-11 in CDW.

The spatial pattern of deep ventilation in the Southern Ocean is shown in Figure 9, which features CFC-11 concentrations near 3 km depth for the five cases during 1983. Clearly evident in all cases are two major sources of deep/bottom water, namely the Ross and Weddell Seas. Subtle differences between the patterns for CTRL, AAS, and NAW primarily reflect shifts in the pattern of deep convection between the runs. The markedly enhanced spread of low values of CFC concentration away from the source regions in case ISOP is apparent in Figure 9d. Case GM (Figure 9e) features deep ventilation that is much weaker than in all the other runs. This weakness reflects the absence of deep convection, the weakness of meridional overturning, and the very limited access of isopycnal tracer diffusion to the deep neutral surfaces from the ocean surface.

6.3. CFC Uptake in the North Atlantic Ocean

Detectable levels of dissolved CFC-11 were first measured in the Deep Western Boundary Current (DWBC) of the North Atlantic Ocean by Weiss *et al.* [1985] (see Figure 10a). Their measurements confirm the presence of CFC-enriched waters at the western boundary of the tropical Atlantic Ocean, with equatorial CFC-11 concentrations reaching 0.05 pmol kg⁻¹ near 1600 m depth by early 1983. The corresponding maps of simulated CFC-11 concentration in the DWBC in four of the model experiments are included in Figure 10. The AAS case is almost

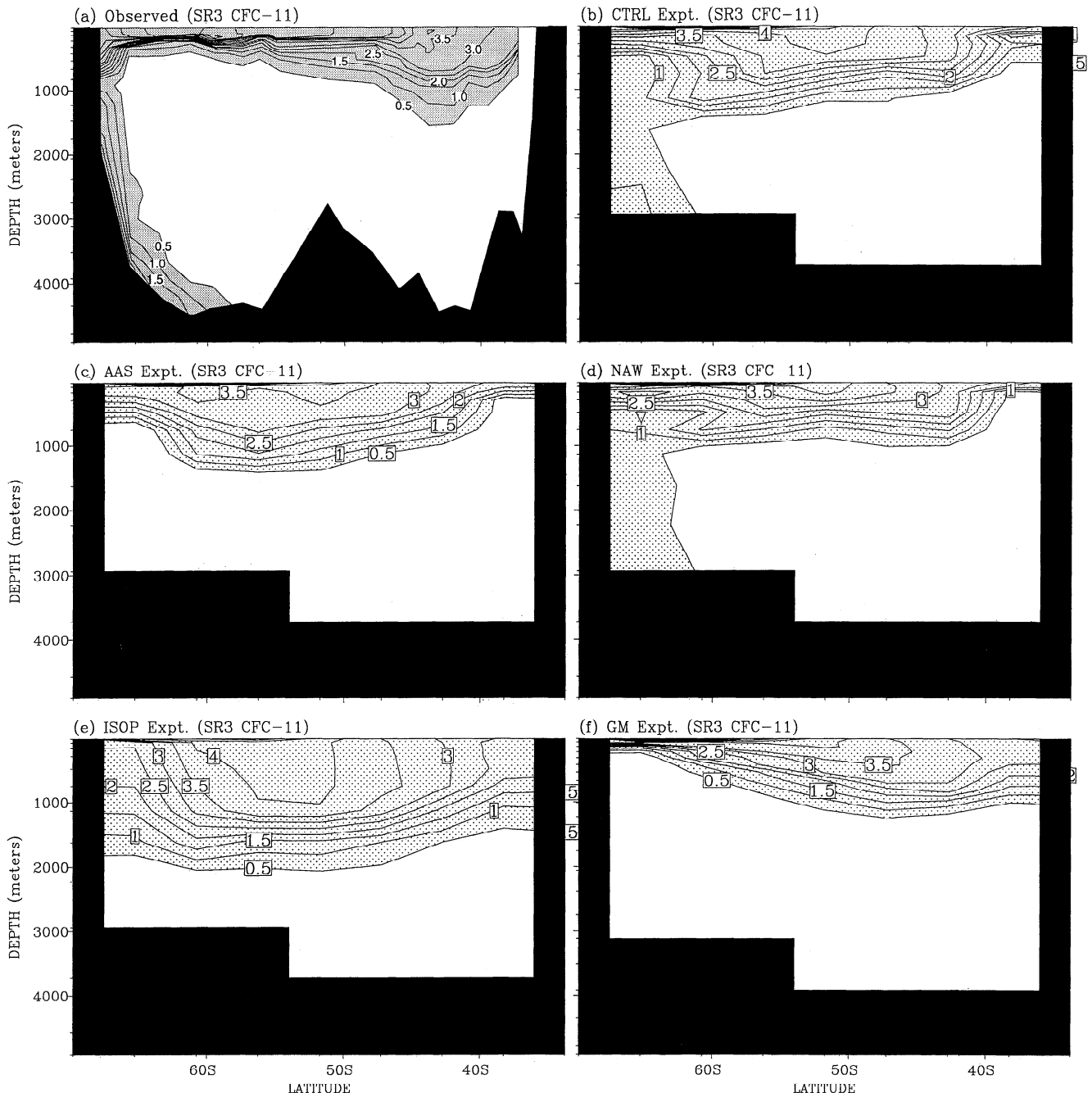


Figure 8. Latitude-depth sections of dissolved CFC-11 along WOCE section SR3 across the Southern Ocean at approximately 150°E during 1991. (a) Observed (data provided courtesy of J. L. Bullister) and (b)-(f) experiments CTRL, AAS, NAW, ISOP, and GM. Contour levels are drawn at intervals of 0.5 pmol kg⁻¹.

indistinguishable from the CTRL experiment and is therefore not shown. The CFC data are sampled from the model ocean during early 1983, in order to correspond with the equivalent measurements made by *Weiss et al.* [1985]. The maps are chosen on those geopotential surfaces that coincide with the core of the DWBC in each case, which varies in depth from 1228 m (experiment GM) to 2228 m (experiment NAW). This is more appropriate than choosing the same density level as that selected by *Weiss et al.* [1985] since the model deep water masses are generally less dense than observed. In addition, the *Weiss et al.* [1985] density surface was selected to cut through the core of the maximum CFC signal in the DWBC.

Except for the NAW case, the model runs exhibit much weaker CFC-11 concentrations in the western boundary outflow compared with observations. In effect, the model southward extension of CFC-enriched upper NADW does not match observations in experiments CTRL, AAS, ISOP, and GM. Unlike the observed section, no deep signal of CFC-11 (in excess of 0.015 pmol kg⁻¹) is seen near the equator off South America in experiments CTRL, AAS, and GM, and in experiment ISOP the deep signal is not restricted to the DWBC due to excessive mixing in that case. The DWBC is deficient in CFC-11 in these four model cases because the timescale for NADW outflow is too slow. The long timescale is primarily due to un-

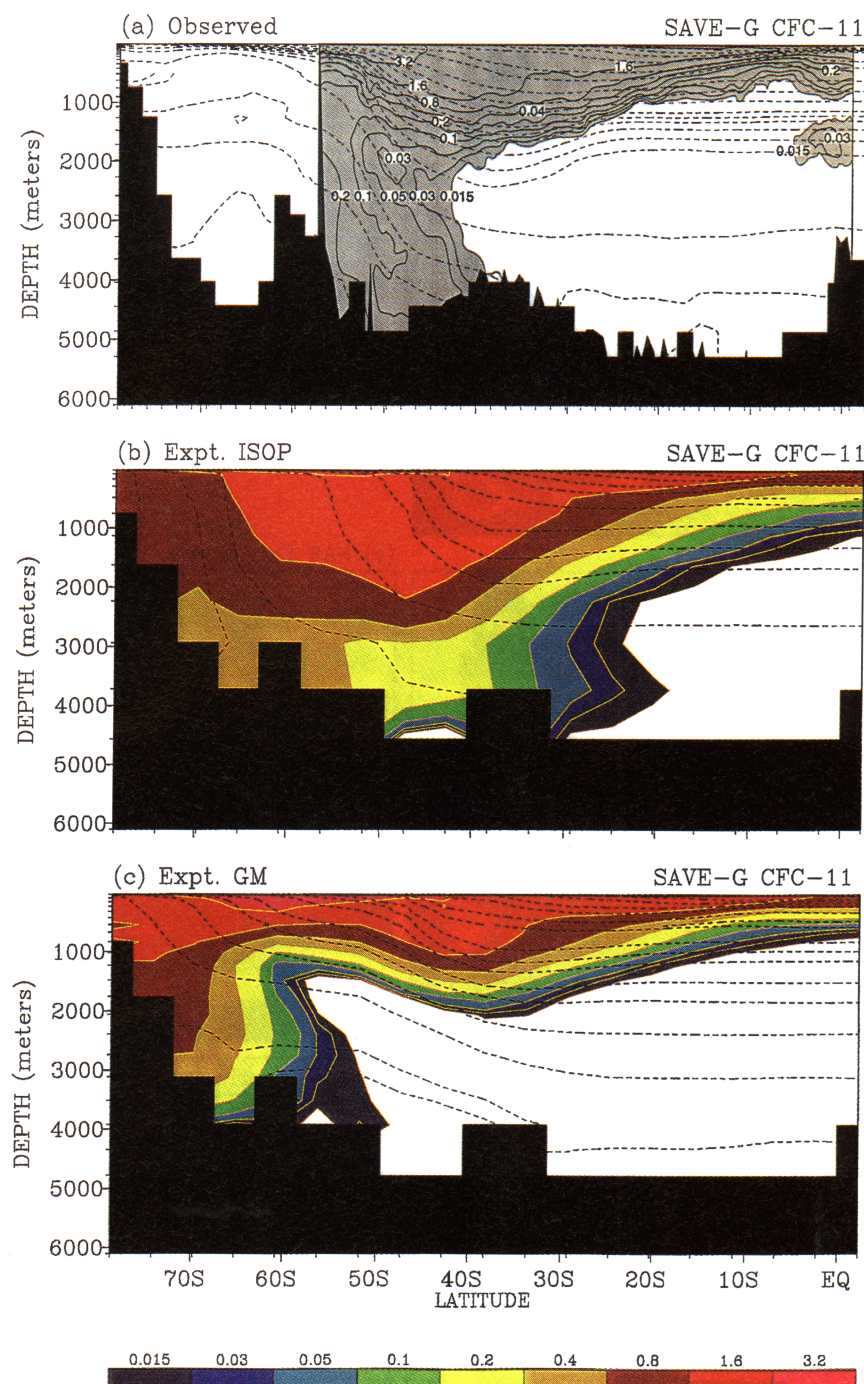


Plate 2. Observed and modeled CFC-11 along the SAVE-G transect in the South Atlantic near 25°W-35°W (January-April, 1989) superposed on estimates of the trajectories followed by isopycnal tracer diffusion. For the purposes of this diagram the SAVE-G section (which was taken southward to 55°S [Weiss *et al.*, 1993]) is extended southwestward into the Weddell Sea for the model cases. No CFC data can therefore be presented south of 55°S in the observed panel. The neutral surface trajectories are estimated following the method of Reid [1981, 1989] as in Plate 1. The neutral surfaces overlaying the observed SAVE-G CFC-11 section are derived from the Levitus [1982] climatology of the World Ocean.

realistically sluggish deep currents, particularly in the GM case (Figure 10e). In addition, in all model runs, part of the path of NADW outflow includes a questionable loop eastward from the Labrador Sea into the Northeastern Atlantic Basin, effectively increasing the required outflow journey by around 4000 km [England *et al.*, 1994]. The additional circulation eastward ages the water mass by at least 8 years (depending on

the speed of the model ocean currents), thereby yielding significantly lower CFC concentrations in the NADW extension.

The outflowing CFC-11 signal is far too diffuse in the isopycnal mixing experiment (Figure 10d), having little zonal structure even though the outflow currents are predominantly at the western boundary. Model data sampled during later years confirms that all other experiments simulate an outflowing

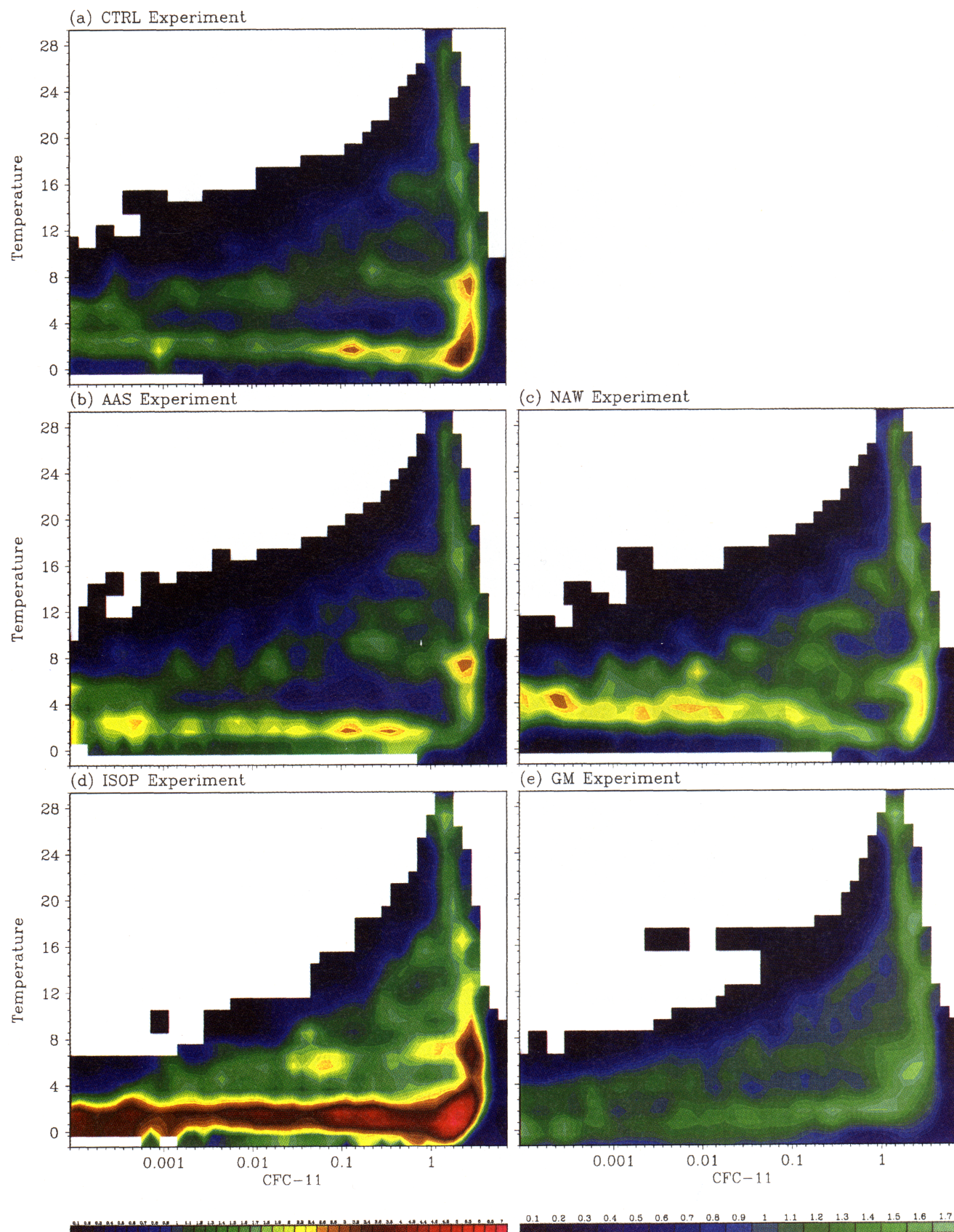


Plate 3. A volumetric census of water in the World Ocean as a function of CFC-11 content and potential temperature for each of the five experiments during 1994. The volumetric census is performed by binning water masses over a mesh with a linear 1°C incrementation in temperature and a logarithmic scale for CFC-11. Units are 10^6 km^3 .

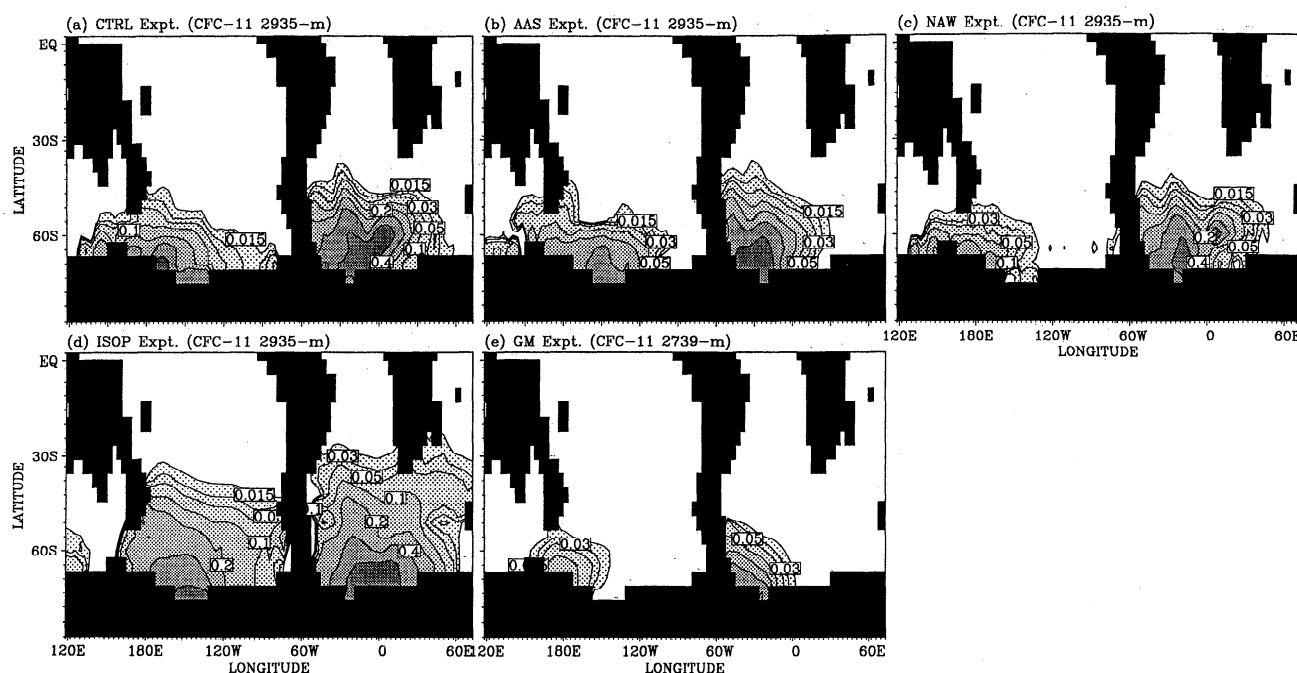


Figure 9. Concentration of dissolved CFC-11 at 2935 m depth (model level 10) during late 1983 in runs CTRL, AAS, NAW, and ISOP. Also included is the corresponding horizontal section at the nearest depth level in case GM (2739 m depth). Contour levels are drawn at 0.015, 0.03, 0.05, 0.1, 0.2, 0.4, 0.8, and 1.6 pmol kg⁻¹.

signal along the western boundary of the deep tropical Atlantic, whereas the isopycnal mixing case diffuses much of this signal eastward. The inclusion of an isopycnal mixing scheme without a substantial reduction in background horizontal mixing can therefore introduce significant errors in the simulated ventilation of the ocean model in the North Atlantic.

The GM experiment shows a great reduction in model ocean current speeds in the DWBC, with the current decreasing in strength from typically 2.0 cm s⁻¹ (CTRL) to 1.0–1.5 cm s⁻¹ (GM). This decrease in flow speed is likely to be due to flattened isopycnal surfaces in the GM runs which act to reduce the strength of interior geostrophic flows. This reduces the speed of flow in the DWBC in an already viscous model with sluggish deep currents. A spatially varying coefficient for the GM isopycnal thickness diffusion term such as that advocated by Visbeck *et al.* [1997] - one that depends on vertical and horizontal stratification - might yield substantially different baroclinic currents in the region. Additional experiments with a spatially varying GM isopycnal thickness diffusion coefficient are recommended.

The net meridional overturning in the North Atlantic is generally shallower and weaker in the GM case, although there is a reduction in the spurious western boundary upwelling as noted by Böning *et al.* [1995]. Even when the GM case was rerun with an enhanced wintertime T-S restoration (as in experiment NAW), the outflowing CFC-11 signal is still markedly weaker than what Weiss *et al.* [1985] observe (Figure 10f).

The enhanced wintertime T-S restoration in experiment NAW increases the production rate of NADW to 28.5 Sv (from 20.1 Sv in the CTRL); and the outflow transport also increases (from 8.5 Sv in CTRL to 17.3 Sv in NAW, Table 3). Correspondingly, the CFC-11 burden in the outflowing NADW is enhanced, with a clear signal in the western boundary current off South America by 1983 (Figure 10c). The core of the outflowing CFC signal has deepened from 1622 m (CTRL) to

2228 m (NAW), with more direct flow of CFC-enriched Labrador Sea Water (LSW) flowing southward from the convection zone (instead of looping eastward into the northeastern Atlantic Basin). This has the net effect of enhancing the CFC-11 content in the DWBC in broad agreement with the observed sections of Weiss *et al.* [1985]. However, as noted earlier, our technique of enhancing the T-S restoring terms implies unrealistically large heat and freshwater fluxes in the North Atlantic during winter. In effect, the model circulation is being corrected using artificial surface forcing fields.

In a model experiment identical to CTRL though including the Eby and Holloway [1994] parameterization of topographic stress, England and Holloway [1997] have shown that the speed of the DWBC intensifies and less LSW flows eastward toward the northeastern Atlantic Basin than in the CTRL run. They show that the CFC simulation improves in the DWBC in the topographic stress case, with a narrower and more enriched CFC-11 signal off South America by early 1983.

6.4. Volumetric Analysis of CFC Uptake

The CFC simulations can be analyzed in terms of the total volume of ocean ventilated by different concentrations of CFC-11. It is useful to map this as a function of potential temperature as well, to further distinguish water masses according to location in the ocean. Plate 3 shows a volumetric census of water in the World Ocean as a function of CFC-11 content and potential temperature for each of the five experiments during 1994. The volumetric census is performed by binning water masses over a mesh with a linear 1°C incrementation in temperature and a logarithmic scale for CFC-11. A substantial volume of deep water in the Pacific and Indian Oceans remains CFC-free by 1994. Such water masses do not contribute to the volumetric census (which ignores water with CFC-11 concentration weaker than 10⁻⁴ pmol kg⁻¹). Much of the CFC-venti-

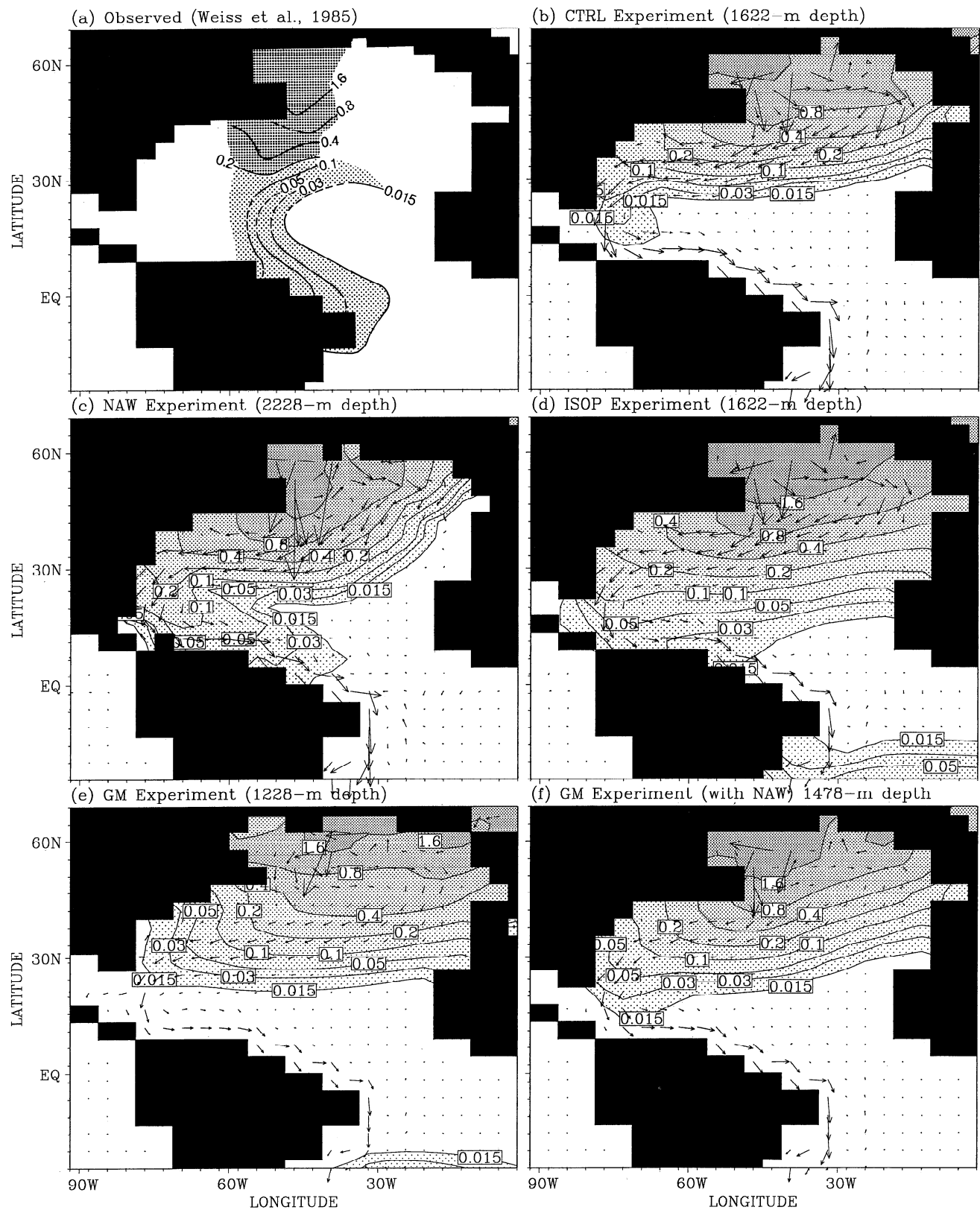


Figure 10. (a) Observed concentration of dissolved CFC-11 in the core of Upper NADW outflow measured during December 1982 to February 1983 as part of the Transient Tracers in the Ocean (TTO) Program (redrafted from Weiss *et al.* [1985]). (b)-(e) Simulated model currents and the concentration of dissolved CFC-11 at the depth level of maximum CFC content in the DWBC during February 1983. Contour levels are drawn at the standard concentrations. Experiment AAS is virtually identical to CTRL and so is not shown. (f) The corresponding map from the GM case when a thermohaline forcing is adopted with tightly constrained wintertime North Atlantic conditions (as in experiment NAW).

lated interior water has temperature in the range 1°–6°C, and so most of the CFC-temperature census falls into this domain. Substantial differences are noted between the five model cases.

In the control experiment there is a clear maximum in the volumetric analysis at around 2–3°C and 1–3 pmol kg⁻¹. Much of this CFC-burdened water is the model equivalent of CDW, which is normally observed to be relatively depleted in CFC. The major volumes of water on the θ -CFC map include a signal of deep water (at 1°–3°C) with a range of CFC concentrations, bottom water (with temperatures less than 1°C), and a trace of intermediate water ventilation at temperatures of 5°–7°C. Thermocline water ventilation is seen at temperatures of around 10°–15°C.

The contribution of AABW to the volumetric map can be thought of as occupying the colder end of the diagram, with high CFC concentration water (on the lower right-hand corner of the diagrams) representing newly-formed bottom water. In experiment AAS, more CFC-11 is detected in the bottom waters of the model, though weaker CFC-11 content is seen in the deep water (with a spread of the maximum signal in CTRL deep water over a range of weaker concentrations in AAS). Intermediate and thermocline water ventilation appears largely unchanged from experiment CTRL.

In experiment NAW, bottom waters are less burdened with CFC compared with CTRL, though there is now an enhanced volume of deep water bearing detectable levels of CFC-11 (because of enhanced ventilation of NADW in that run).

A dramatic increase in CFC ventilation is noted in the ISOP experiment. Bottom, deep, and intermediate water burdens of CFC-11 are all substantially higher in ISOP than in all the other cases, particularly the signal corresponding to CDW. This reflects the strong mixing and more rapid blending of water masses in that run. In contrast, experiment GM exhibits relatively weak CFC burdens in all the major water masses, consistent with the reduced convection, meridional overturning, and tracer mixing in that model run.

7. Summary and Conclusions

In this study we have examined the role of surface thermohaline forcing and subsurface mixing parameterization in determining the nature of ocean ventilation in general circulation models. In particular, a series of five model experiments were forced with the same air-sea CFC flux condition, but with different surface thermohaline forcing and/or subsurface mixing parameterization. The standard CFC forcing matches the most realistic case considered in part 1 of this study, namely, the air-sea exchange is a function of local wind speed and sea-ice coverage, as well as the Schmidt number of the given gas. The cycling of atmospheric CFC-11 and CFC-12 solubilities (as a function of sea surface temperature and salinity) is controlled in the five cases by referencing the seasonal climatology rather than the model ocean simulations.

The five ocean states included (1) a control run with a standard seasonal cycle in surface forcing and traditional Cartesian mixing (CTRL), (2) a run in which the production rate and salinity of Antarctic Bottom Water is increased (AAS), (3) a run in which the production, outflow rates, and density of North Atlantic Deep Water is increased (NAW), (4) a run with enhanced isopycnal mixing of passive tracers (ISOP), and, finally, (5) a run in which the effects of eddies on the mean ocean flow are parameterized following *Gent et al.* [1995] (GM). The changes in deep/bottom water ventilation rates in

runs (2) and (3) were effected by changes in surface thermohaline forcing off Antarctica and in the North Atlantic Ocean, respectively.

The simulated CFC uptake in the Southern Ocean was seen to exceed observations in all experiments except run GM. The uptake is particularly excessive in cases CTRL and ISOP. The spurious uptake of CFC was found to be directly related to poor reproduction of the Southern Ocean water mass structure, in particular, insufficient stratification south of 50°S and excessively buoyant deep water. The insufficient density of Circumpolar Deep Water allows for extensive penetration of convective adjustment to great depth during winter, in contrast to observations, and this drives excessive downward mixing of the CFC-enriched surface waters. Compared with the control experiment, the Southern Ocean CFC uptake is reduced in the cases with increased AABW salinity and NADW density, as a result of slightly higher deep water density and reduced wintertime convection in those experiments. Nevertheless, CFC uptake in the Southern Ocean still exceeds observed ocean CFC content in the adjusted surface forcing cases. In addition, unrealistic surface heat (NAW) and freshwater (AAS) fluxes are required in these runs to satisfy the wintertime surface restoring conditions.

The most extreme uptake occurs in experiment ISOP where, in addition to deep convective mixing of CFC, there is also mixing into the ocean interior along isopycnal surfaces having an unrealistic orientation. The Southern Ocean CFC uptake in GM, using the mixing scheme of *Gent et al.* [1995] and zero horizontal diffusion, is dramatically reduced over that in the other runs. Only in this run do deep densities approach the observed values, and wintertime convection is largely suppressed south of the Antarctic Circumpolar Current. Deep penetration of CFC-rich water occurs only in the western Weddell and Ross Seas. One of the major achievements of the GM case is to simulate relatively depleted levels of CFC in the model equivalent of Circumpolar Deep Water. This run yields CFC sections in the Southern Ocean which compare most favorably with observations. Nevertheless, substantial model-observation differences exist even under GM, such as too slow a ventilation rate of AABW and unresolved downslope flows at certain locations (e.g., SR3, Figure 8). It seems that in spite of the demonstrated improvements noted under this scheme, there may be an *a priori* limit in the capability of coarse-resolution ocean models to simulate the net effect of small-scale processes, such as shelf-driven deep water formation and downslope flows.

The simulation of NADW production was found to be problematic in all runs, with the CFC signature indicating primary source regions in the Labrador Sea and immediately to the southeast of Greenland, while the Norwegian-Greenland Sea overflow water (which is dominant in reality) plays only a minor role. Lower NADW is insufficiently dense in all runs, and outflow currents in the deep western boundary current are too weak (especially in case GM due to flattened isopycnal surfaces). Only in the run with surface forcing designed to enhance NADW production does the CFC signal penetrate down the western Atlantic boundary in a realistic manner. However, this case implies an unrealistic net ocean surface heat loss adjacent to Greenland and so cannot be advocated as a technique to improve model NADW production.

Meridional depth sections and volumetric maps of CFC concentration indicate that on the timescales resolved by CFC uptake, the dominant determining factor in overall model venti-

lation is the choice of subsurface mixing scheme. The surface thermohaline forcing determines more subtle aspects of the subsurface CFC content. This means that the choice of sub-grid-scale mixing scheme plays a key role in determining ocean model ventilation over decadal to centennial timescales. This has important implications for climate model studies. Future work should be directed at examining CFC uptake in a range of models adopting different subsurface mixing coefficients and mixing schemes, particularly those used within coupled atmosphere-ocean-ice models of the climate system.

Acknowledgments. The model computations were carried out on the CSIRO Cray-YMP 4E/369 and the UNSW Cray YMP-EL. This research was supported by the ARC Small Grants Scheme and EPOCH CEE grant EVSV CT92/0124, and was initiated in collaboration with Véronique Garçon and Jean-François Minster while MHE was at GRGS/CNRS. This study contributes to the CSIRO Climate Change Research Program and was partly funded through Australia's National Greenhouse Research Program. Trevor McDougall and two anonymous reviewers made valuable comments on the original manuscript. MHE further acknowledges support from the University of New South Wales Vice-Chancellor's Research Fellowship Scheme.

References

- Akitomo, K., T. Awaji, and N. Imasato, Open ocean deep convection in the Weddell Sea: Two-dimensional numerical experiments with a nonhydrostatic model, *Deep Sea Res.*, 42, 53-73, 1995.
- Böning, C.W., W.R. Holland, F.O. Bryan, G. Danabasoglu, and J.C. McWilliams, An overlooked problem in model simulations of the thermohaline circulation and heat transport in the Atlantic Ocean, *J. Clim.*, 8, 515-523, 1995.
- Bryan, K., A numerical method for the study of the circulation of the World Ocean, *J. Comput. Phys.*, 3, 347-376, 1969.
- Bryan, K., and L.J. Lewis, A water mass model of the World Ocean, *J. Geophys. Res.*, 84, 2503-2517, 1979.
- Bullister, J.L., Chlorofluorocarbons as time-dependent tracers in the ocean, *Oceanography*, 2, 12-17, 1989.
- Comiso, J.C., C.R. McClain, C.W. Sullivan, J.P. Ryan, and C.L. Leonard, Coastal zone color scanner pigment concentrations in the Southern Ocean and relationships to geophysical surface features, *J. Geophys. Res.*, 98, 2419-2451, 1993.
- Cox, M.D., A primitive equation, three-dimensional model of the ocean, *Tech. Rep. 1*, 143 pp., Geophys. Fluid Dyn. Lab. Ocean Group, Princeton, N.J., 1984.
- Cox, M.D., An idealised model of the World Ocean, 1, The global scale water masses, *J. Phys. Oceanogr.*, 19, 1730-1752, 1989.
- Cubasch, U., K. Hasselmann, H. Hock, E. Maier-Reimer, U. Mikolajewicz, B.D. Santer, and R. Sausen, Time dependent greenhouse warming computations with a coupled ocean-atmosphere model, *Clim. Dyn.*, 8, 55-69, 1992.
- Cummins, P.F., G. Holloway, and A.E. Gargett, Sensitivity of the GFDL ocean model to a parameterization of vertical diffusion, *J. Phys. Oceanogr.*, 20, 817-830, 1990.
- Danabasoglu, G., and J.C. McWilliams, Sensitivity of the global ocean circulation to parameterizations of mesoscale tracer transports, *J. Clim.*, 8, 2967-2987, 1995.
- Danabasoglu, G., J.C. McWilliams, and P.R. Gent, The role of mesoscale tracer transports in the global ocean circulation, *Science*, 264, 1123-1126, 1994.
- Dixon, K.W., J.L. Bullister, R.H. Gammon, and R.J. Stouffer, Examining a coupled climate model using CFC-11 as an ocean tracer, *Geophys. Res. Lett.*, 23, 1957-1960, 1996.
- Döscher, R., C.W. Böning, and P. Herrmann, Response of meridional overturning and heat transport in the North Atlantic to changes in thermohaline forcing at northern latitudes: A model study, *J. Phys. Oceanogr.*, 24, 2306-2320, 1994.
- Duffy, P.B., D. Eliason, A.J. Bourgeois, and C. Covey, Simulation of bomb radiocarbon in two ocean general circulation models, *J. Geophys. Res.*, 100, 22,545-22,565, 1995.
- Eby, M., and G. Holloway, Sensitivity of a large-scale ocean model to a parameterization of topographic stress, *J. Phys. Oceanogr.*, 24, 2577-2588, 1994.
- Elkins, J.W., T.M. Thompson, T.H. Swanson, J.H. Butler, B.D. Hall, S.O. Cummings, D.A. Fisher, and A.G. Raffo, Decrease in the growth rates of atmospheric chlorofluorocarbons 11 and 12, *Nature*, 364, 780-783, 1993.
- England, M.H., On the formation of Antarctic Intermediate and Bottom Water in ocean general circulation models, *J. Phys. Oceanogr.*, 22, 918-926, 1992.
- England, M.H., Representing the global-scale water masses in ocean general circulation models, *J. Phys. Oceanogr.*, 23, 1523-1552, 1993.
- England, M.H., Using chlorofluorocarbons to assess ocean climate models, *Geophys. Res. Lett.*, 22, 3051-3054, 1995.
- England, M.H., and G. Holloway, Simulations of CFC-11 outflow and seawater age in the Deep North Atlantic, in *Applications of Trace Substance Measurements to Oceanographic Problems*, edited by P. Schlosser, W.M. Smethie, and J.R. Toggweiler, AGU, Washington, D. C., in press, 1997.
- England, M.H., V.C. Garçon, and J.-F. Minster, Chlorofluorocarbon uptake in a World Ocean model, 1, Sensitivity to the surface gas forcing, *J. Geophys. Res.*, 99, 25,215-25,233, 1994.
- Esbenson, S.K., and Y. Kushnir, The heat budget of the global ocean: An atlas based on estimates from surface marine observations, *Rep. 29*, Clim. Res. Inst., Oreg. State Univ., Corvallis, Oregon, 1981.
- Fine, R.A., Circulation of Antarctic Intermediate Water in the South Indian Ocean, *Deep Sea Res.*, 40, 2021-2042, 1993.
- Gent, P.R., and J.C. McWilliams, Isopycnal mixing in ocean circulation models, *J. Phys. Oceanogr.*, 20, 150-155, 1990.
- Gent, P.R., J. Willebrand, T.J. McDougall, and J.C. McWilliams, Parameterizing eddy-induced tracer transports in ocean circulation models, *J. Phys. Oceanogr.*, 25, 463-474, 1995.
- Gordon, H.B., and S.P. O'Farrell, Transient climate change in the CSIRO coupled model with dynamic sea ice, *Mon. Weather Rev.*, 125, 875-907, 1997.
- Hellerman, S., and M. Rosenstein, Normal monthly wind stress over the World Ocean with error estimates, *J. Phys. Oceanogr.*, 13, 1093-1104, 1983.
- Hirst, A.C., and W. Cai, Sensitivity of a World Ocean GCM to changes in subsurface mixing parameterization, *J. Phys. Oceanogr.*, 24, 1256-1279, 1994.
- Hirst, A.C., and T.J. McDougall, Deep water properties and surface buoyancy flux as simulated by a z-coordinate model including eddy-induced advection, *J. Phys. Oceanogr.*, 26, 1320-1343, 1996.
- Hirst, A.C., D. Jackett, and T.J. McDougall, The meridional overturning cells of a World Ocean model in neutral surface coordinates, *J. Phys. Oceanogr.*, 26, 775-791, 1996.
- Jacobs, S.S., R.G. Fairbanks, and Y. Horibe, Origin and evolution of water masses near the Antarctic continental margin: Evidence from $H_2^{18}O/H_2^{16}O$ ratios in seawater, in *Oceanology of the Antarctic Continental Shelf*, *Antarct. Res. Ser.*, vol. 43, edited by S.S. Jacobs, pp. 58-86, AGU, Washington, D. C., 1985.
- Killworth, P.D., Deep convection in the World Ocean, *Rev. Geophys.*, 21, 1-26, 1983.
- Levitus, S., Climatological atlas of the World Ocean, *NOAA Prof. Pap. 13*, 173 pp., U.S. Dep. of Commer., Washington, D. C., 1982.
- Manabe, S., and R.J. Stouffer, Multiple-century response of a coupled ocean-atmosphere model to an increase of atmospheric carbon dioxide, *J. Clim.*, 7, 5-23, 1994.
- Manabe, S., R.J. Stouffer, M.J. Spelman, and K. Bryan, Transient responses of a coupled ocean-atmosphere model to gradual changes of atmospheric carbon dioxide, 1, Annual mean response, *J. Clim.*, 4, 785-818, 1991.
- Manabe, S., M.J. Spelman, and R.J. Stouffer, Transient responses of a coupled ocean-atmosphere model to gradual changes of atmospheric carbon dioxide, 2, Seasonal response, *J. Clim.*, 5, 105-126, 1992.
- McCartney, M.S., Subantarctic Mode Water, *Deep Sea Res.*, 24, suppl., 103-119, 1977.
- McDougall, T.J., Neutral surfaces, *J. Phys. Oceanogr.*, 17, 1950-1964, 1987.
- McDougall, T.J., and J.A. Church, Pitfalls with the numerical representation of isopycnal and diapycnal mixing, *J. Phys. Oceanogr.*, 16, 196-199, 1986.
- McDougall, T.J., and P.C. McIntosh, The temporal-residual-mean velocity, 1, Derivation and the scalar conservation equations, *J. Phys. Oceanogr.*, 26, 2653-2665, 1996.
- McDougall, T.J., A.C. Hirst, M.H. England, and P.C. McIntosh,

- Implications of a new eddy parameterization for ocean models, *Geophys. Res. Lett.*, **23**, 2085-2088, 1996.
- Molina, M.J., and F.S. Rowland, Stratospheric sink for chlorofluoromethanes: Chlorine atom catalysed destruction of ozone, *Nature*, **249**, 810-812, 1974.
- Nowlin, W.D., and J.M. Klinck, The physics of the Antarctic Circumpolar Current, *Rev. Geophys.*, **24**, 469-491, 1986.
- Olbers, D., V. Gouretzki, G. Seiß, and J. Schroeter, *The Hydrographic Atlas of the Southern Ocean*, Alfred-Wegener-Inst. for Polar and Mar. Res., Bremerhaven, Germany, 1992.
- Pacanowski, R.C., K.W. Dixon, and A. Rosati, The GFDL Modular Ocean Model Users Guide version 1.0, *Tech. Rep. 2*, 46 pp., Geophys. Fluid Dyn. Lab. Ocean Group, Princeton, N.J., 1991.
- Parkinson, C.L., J.C. Comiso, H.J. Zwally, D.J. Cavalieri, P. Gloersen, and W.J. Campbell, Arctic sea ice, 1973-1976: Satellite passive-microwave observations, *NASA Spec. Publ. SP 489*, 296 pp., 1987.
- Redi, M.H., Oceanic isopycnal mixing by coordinate rotation, *J. Phys. Oceanogr.*, **12**, 1154-1158, 1982.
- Reid, J.L., On the mid-depth circulation of the World Ocean, in *Evolution of Physical Oceanography*, edited by B.A. Warren and C. Wunsch, pp. 70-111, MIT Press, Cambridge, MA, and London, England, 1981.
- Reid, J.L., On the total geostrophic circulation of the South Atlantic Ocean: Flow patterns, tracers and transports, *Progr. Oceanogr.*, **23**, 149-244, 1989.
- Rhein, M., Ventilation rates of the Greenland and Norwegian Seas derived from distributions of the chlorofluoromethanes F11 and F12, *Deep Sea Res.*, **38**, 485-503, 1991.
- Rintoul, S.R., South Atlantic interbasin exchange, *J. Geophys. Res.*, **96**, 2675-2692, 1991.
- Rix, N.H., and J. Willebrand, A note on the parameterization of mesoscale eddies as inferred from a high resolution circulation model, *J. Phys. Oceanogr.*, **26**, 2281-2285, 1996.
- Robitaille, D.Y., and A.J. Weaver, Validation of subgrid-scale mixing schemes using CFCs in a global ocean model, *Geophys. Res. Lett.*, **22**, 2917-2920, 1995.
- Roether, W., R. Schlitzer, A. Putzka, P. Beining, K. Bulsiewicz, G. Rohardt, and F. Delahoyde, A chlorofluoromethane and hydrographic section across Drake Passage: Deep water ventilation and meridional property transport, *J. Geophys. Res.*, **98**, 14,423-14,435, 1993.
- Schlosser, P., J.L. Bullister, and R. Bayer, Studies of deep water formation and circulation in the Weddell Sea using natural and anthropogenic tracers, *Mar. Chem.*, **35**, 97-122, 1991.
- Schmitz, W.J., On the interbasin-scale thermohaline circulation, *Rev. Geophys.*, **33**, 151-173, 1995.
- Smethie, W.M., Tracing the thermohaline circulation in the western North Atlantic using chlorofluorocarbons, *Prog. Oceanogr.*, **31**, 51-99, 1993.
- Stouffer, R.J., S. Manabe, and K. Bryan, Interhemispheric asymmetry in climate response to a gradual increase of atmospheric CO₂, *Nature*, **342**, 660-662, 1989.
- Toggweiler, J.R., and B. Samuels, Effect of sea ice on the salinity of Antarctic Bottom Waters, *J. Phys. Oceanogr.*, **25**, 1980-1997, 1995.
- Toggweiler, J.R., K. Dixon, and K. Bryan, Simulations of radiocarbon in a coarse-resolution world ocean model, 1, Steady state prebomb distributions, *J. Geophys. Res.*, **94**, 8217-8242, 1989.
- Trumbore, S.E., S.S. Jacobs, and W.M. Smethie, Chlorofluorocarbon evidence for rapid ventilation of the Ross Sea, *Deep Sea Res.*, **38**, 845-870, 1991.
- Veronis, G., The role of models in tracer studies, in *Numerical Models of the Ocean Circulation*, pp. 133-146, Nat. Acad. of Sci., Washington, D. C., 1975.
- Visbeck, M., J. Marshall, T. Haine, and M. Spall, On the specification of eddy transfer coefficients in coarse resolution ocean circulation models, *J. Phys. Oceanogr.*, **27**, 381-402, 1997.
- Wallace, D.W.R., and J.R.N. Lazier, Anthropogenic chlorofluoromethanes in newly formed Labrador Sea Water, *Nature*, **332**, 61-63, 1988.
- Wanninkhof, R., Relationship between wind speed and gas exchange over the ocean, *J. Geophys. Res.*, **97**, 7373-7382, 1992.
- Warner, M.J., and R.F. Weiss, Solubilities of chlorofluorocarbons 11 and 12 in water and seawater, *Deep Sea Res.*, **32**, 1485-1497, 1985.
- Warner, M.J., and R.F. Weiss, Chlorofluoromethanes in South Atlantic Antarctic Intermediate Water, *Deep Sea Res.*, **39**, 2053-2075, 1992.
- Weiss, R.F., J.L. Bullister, R.H. Gammon, and M.J. Warner, Atmospheric chlorofluoromethanes in the deep equatorial Atlantic, *Nature*, **314**, 608-610, 1985.
- Weiss, R.F., M.J. Warner, P.K. Salamch, F.A. Van Woy, and K.G. Harrison, South Atlantic Ventilation Experiment: SIO chlorofluorocarbon measurements, *Scripps Inst. Oceanogr. Ref. 93-49*, 466 pp., Scripps Inst. of Oceanogr., La Jolla, Calif., 1993.
- Whetton, P., M.H. England, S.P. O'Farrell, I.G. Watterson, and A.B. Pittock, Global comparison of the regional rainfall results of enhanced greenhouse coupled and mixed layer ocean experiments: Implications for climate change scenario development, *Clim. Change*, **33**, 497-519, 1996.
- Wu, X., I. Simmonds, and W.F. Budd, Modeling of Antarctic sea ice in a general circulation model, *J. Clim.*, **10**, 593-609, 1997.
- Zwally, H.J., J.C. Comiso, and A.L. Gordon, Antarctic offshore leads and polynyas and oceanographic effects, in *Oceanology of the Antarctic Continental Shelf*, *Antarct. Res. Ser.*, vol. 43, edited by S.S. Jacobs, pp. 203-226, AGU, Washington, D. C., 1985.

M. H. England (corresponding author), School of Mathematics, University of New South Wales, NSW 2052, Australia. (e-mail: M.England@unsw.edu.au)

A. C. Hirst, Division of Atmospheric Research, CSIRO, PMB 1, Aspendale, 3195, Victoria, Australia. (e-mail: ach@dar.csiro.au)

(Received July 31, 1996; revised December 31, 1996; accepted January 16, 1997.)